



UNIVERSITY OF LEEDS

This is a repository copy of *Kinetics of CH₂OO reactions with SO₂, NO₂, NO, H₂O and CH₃CHO as a function of pressure.*

White Rose Research Online URL for this paper:
<http://eprints.whiterose.ac.uk/121551/>

Version: Accepted Version

Article:

Stone, D orcid.org/0000-0001-6710-4021, Blitz, M, Daubney, L et al. (2 more authors) (2014) Kinetics of CH₂OO reactions with SO₂, NO₂, NO, H₂O and CH₃CHO as a function of pressure. *Physical Chemistry Chemical Physics*, 16 (3). pp. 1139-1149. ISSN 1463-9076

<https://doi.org/10.1039/C3CP54391A>

© the Owner Societies 2014. This is an author produced version of a paper published in *Physical Chemistry Chemical Physics*. Uploaded in accordance with the publisher's self-archiving policy.

Reuse

Items deposited in White Rose Research Online are protected by copyright, with all rights reserved unless indicated otherwise. They may be downloaded and/or printed for private study, or other acts as permitted by national copyright laws. The publisher or other rights holders may allow further reproduction and re-use of the full text version. This is indicated by the licence information on the White Rose Research Online record for the item.

Takedown

If you consider content in White Rose Research Online to be in breach of UK law, please notify us by emailing eprints@whiterose.ac.uk including the URL of the record and the reason for the withdrawal request.



eprints@whiterose.ac.uk
<https://eprints.whiterose.ac.uk/>

Kinetics of CH₂OO reactions with SO₂, NO₂, NO, H₂O and CH₃CHO as a function of pressure

Daniel Stone,^a Mark Blitz,^{a,b*} Laura Daubney,^a Neil Howes,^a Paul Seakins^{a,b}

^a School of Chemistry, University of Leeds, Leeds, UK

^b National Centre for Atmospheric Science, University of Leeds, Leeds, UK

Email: m.blitz@leeds.ac.uk

Abstract

Kinetics of CH₂OO Criegee intermediate reactions with SO₂, NO₂, NO, H₂O and CH₃CHO and CH₂I radical reactions with NO₂ are reported as a function of pressure at 295 K. Measurements were made under pseudo-first-order conditions using flash photolysis of CH₂I₂/O₂/N₂ gas mixtures in the presence of excess co-reagent combined with monitoring of HCHO reaction products by laser-induced fluorescence (LIF) spectroscopy and, for the reaction with SO₂, direct detection of CH₂OO by photoionisation mass spectrometry (PIMS). Rate coefficients for CH₂OO + SO₂ and CH₂OO + NO₂ are independent of pressure in the ranges studied and are $(3.42 \pm 0.42) \times 10^{-11} \text{ cm}^3 \text{ s}^{-1}$ (measured between 1.5 and 450 Torr) and $(1.5 \pm 0.5) \times 10^{-12} \text{ cm}^3 \text{ s}^{-1}$ (measured between 25 and 300 Torr), respectively. The rate coefficient for CH₂OO + CH₃CHO is pressure dependent, with the yield of HCHO decreasing with increasing pressure. Upper limits of $2 \times 10^{-13} \text{ cm}^3 \text{ s}^{-1}$ and $9 \times 10^{-17} \text{ cm}^3 \text{ s}^{-1}$ are placed on the rate coefficients for CH₂OO + NO and CH₂OO + H₂O, respectively. The upper limit for the rate coefficient for CH₂OO + H₂O is significantly lower than has been reported previously, with consequences for modelling of atmospheric impacts of CH₂OO chemistry.

1. Introduction

Criegee intermediates, carbonyl oxide biradicals with the general formula CR₂OO, are principally produced in the atmosphere following ozonolysis of unsaturated volatile organic compounds (VOCs) and are key species in the tropospheric oxidation of both biogenic and anthropogenic compounds.^{1,2} The exothermicity of ozonolysis reactions leads to production of vibrationally excited Criegee intermediates with sufficient energy to undergo unimolecular decomposition to products including OH and HO₂,³⁻⁶ representing a significant source of these important oxidising species in certain important environments.⁷⁻⁹ However, collisional quenching of the nascent excited Criegee intermediate by N₂ or O₂, to produce stabilised Criegee intermediates, is competitive with the unimolecular decomposition processes at ambient pressures,^{1,5} and

reactions of stabilised Criegee intermediates have the potential to impact atmospheric budgets of NO_x ($\text{NO}_x = \text{NO} + \text{NO}_2$), NO_3 , O_3 , HO_x ($\text{HO}_x = \text{OH} + \text{HO}_2$), SO_2 , H_2SO_4 , sulfate aerosol and secondary organic aerosol (SOA).^{5, 10-17}

Despite their potential importance in atmospheric chemistry, and thus in the assessment and prediction of issues such as air quality and climate change, direct observations of Criegee intermediates have only recently been achieved.^{10-12, 18-20} Kinetics and product yields of Criegee intermediate reactions currently used in atmospheric models are subject to large uncertainties, owing to the reliance of previous investigations on indirect techniques involving measurements of stable species in complex ozonolysis experiments, in which there are several potential sources and sinks of the measured species.^{1, 2} Welz *et al.*¹⁰ reported the first direct measurements of Criegee intermediate kinetics, where the photolysis of CH_2I_2 in the presence of O_2 was used to generate the CH_2OO Criegee intermediate at low pressure (4 Torr) and, using synchrotron photoionisation mass spectrometry (PIMS) at the Advanced Light Source (ALS), demonstrated unequivocally that the Criegee intermediate, CH_2OO , was being monitored:



While reactions of CH_2OO with NO and water vapour were reported to be slow, the reactions of CH_2OO with SO_2 and NO_2 were shown to be significantly faster than indicated by the indirect methods. Rate coefficients for both $\text{CH}_2\text{OO} + \text{SO}_2$ and $\text{CH}_2\text{OO} + \text{NO}_2$, measured at a pressure of 4 Torr and temperature of 298 K, were both approximately 1000 times greater than previously assigned, implying a more significant role of Criegee intermediate chemistry in the atmosphere than expected.

The ability to produce CH_2OO following photolysis of CH_2I_2 in the presence of O_2 ¹⁰ has also facilitated spectroscopic investigations of CH_2OO in the infrared¹⁹ and ultraviolet,²⁰ and has been used to demonstrate the production of NO_3 in the reaction of CH_2OO with NO_2 .²¹ Subsequent work at the ALS has investigated the reactions of CH_2OO with acetone, acetaldehyde and hexafluoroacetone at low pressures,¹¹ with theoretical investigation²² of the reaction between CH_2OO and acetaldehyde (CH_3CHO) indicating pressure dependence of the reaction and collisional stabilisation of nascent reaction adducts to produce secondary ozonides (SOZs) at higher pressures which subsequently decompose to generate organic acids.

Taatjes *et al.*¹² have also recently demonstrated production of the CH_3CHOO Criegee intermediate following photolysis of CH_3CHI_2 in the presence of O_2 . The structure of the CH_3CHOO Criegee intermediate gives rise to the possibility of *syn*- and *anti*- conformers, with the conformers sufficiently different in energy, and with a barrier to conversion, leading to the potential for their behaviour as distinct species. Using the synchrotron PIMS technique, Taatjes *et al.*¹² were not only able to identify both the *syn*- and *anti*- CH_3CHOO conformers, but were also able to assign separate rate coefficients for reactions of the two conformers with SO_2 and water vapour. The *anti*-conformer was shown to display greater reactivity

66 towards both SO₂ and H₂O compared to the *syn*-conformer, with rate coefficients for reactions of both *syn*-
67 and *anti*- conformers with SO₂ greater than previously expected.¹²

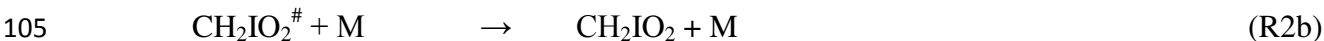
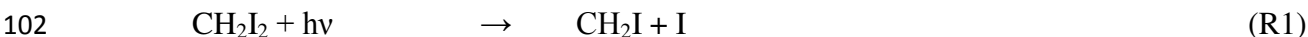
68 Field observations in a boreal forest in Finland have provided further evidence for rapid reactions between
69 Criegee intermediates and SO₂, with measurements identifying the presence of oxidising species other than
70 OH which are able to oxidise SO₂ to SO₃ and ultimately to produce H₂SO₄.²³ The presence of the unknown
71 oxidising species was shown to be related to emissions of biogenic alkenes, and it was postulated that
72 Criegee intermediates may be responsible, with laboratory measurements of H₂SO₄ production during
73 alkene ozonolysis reactions in the presence of SO₂ and OH scavengers providing further support for the
74 action of Criegee intermediates as atmospheric oxidants of SO₂.²³

75 Implementation of increased Criegee intermediate + SO₂ reaction rates in atmospheric models has been
76 shown to improve model simulations of H₂SO₄ in forested regions in Finland and Germany,¹⁴ and global
77 modelling has shown that while global production of H₂SO₄ increases by only 4 %, there are increases of up
78 to 100 % in the boundary layer in tropical forests.¹⁵ Further modelling work has shown that reactions of
79 Criegee intermediates with SO₂ can compete with OH + SO₂ in a number of regions, and that Criegee +
80 SO₂ reactions may be the dominant removal mechanism for SO₂ in certain areas and are major contributors
81 to sulfate aerosol formation on a regional scale.¹⁷ Air quality modelling over the U.S. displayed limited
82 impacts of increased Criegee + SO₂ reaction rates on sulfate aerosol production in this region, but the
83 impacts were shown to be highly dependent on the competition between Criegee + SO₂ and Criegee + H₂O,
84 with a combination of increased Criegee + SO₂ and decreased Criegee + H₂O reaction rates leading to
85 enhanced sulfate aerosol concentrations.¹⁶ However, such studies have largely been based on the low
86 pressure data for CH₂OO + SO₂ reported by Welz *et al.*¹⁰ and there is considerable uncertainty regarding
87 the upper limit for CH₂OO + H₂O.^{2, 17}

88 Theoretical work has provided support for rapid reactions between Criegee intermediates and SO₂,^{13, 24} with
89 reactions proceeding *via* the initial barrierless formation of a cyclic secondary ozonide, and has enabled
90 prediction of potential effects of pressure.¹³ For CH₂OO + SO₂, it has been predicted that the reaction
91 products at atmospheric pressure will be a mixture of HCHO + SO₃ (~68 %), formyl sulfinic ester
92 (HC(O)OS(O)OH) (~15 %) and a singlet bisoxy diradical (CH₂(O)O) + SO₂ (~17 %).¹³ In contrast,
93 reactions of larger Criegee intermediates, including CH₃CHOO, at ambient pressures are expected to result
94 in production of stabilised secondary ozonide species, with little formation of SO₃, and therefore little
95 impact on H₂SO₄ and sulfate aerosol.¹³ Investigation of the reaction products and pressure dependence of
96 Criegee intermediate reactions is thus essential to the accurate determination of their atmospheric impacts.

97 The yield of CH₂OO Criegee intermediates following CH₂I₂ photolysis in O₂ was studied by Huang *et al.*²⁵,
98 and in our previous work,²⁶ as a function of pressure. Both investigations indicate that the initial reaction
99 between CH₂I radicals and O₂ (R2) produce a chemically activated species, CH₂IO₂[#], which decomposes at

100 low pressures to produce $\text{CH}_2\text{OO} + \text{I}$ (R2a), but is also collisionally stabilised at higher pressures to
101 produce the CH_2IO_2 peroxy radical (R2b).



106 Our previous work²⁶ indicates a yield of ~18 % CH_2OO following photolysis of CH_2I_2 in air at 760 Torr,
107 with recent results from Huang *et al.*²⁷ in reasonable agreement. This result has potential significance for
108 modelling of atmospheric chemistry in iodine-rich regions,²⁸⁻³¹ and also indicates potential for pressure
109 dependent studies of CH_2OO kinetics using photolysis of CH_2I_2 in O_2 .

110 In this work, we report kinetics of CH_2OO reactions with SO_2 , NO_2 , NO , H_2O and CH_3CHO at pressures
111 between 25 and 450 Torr at a temperature of 295 K, using photolysis of $\text{CH}_2\text{I}_2/\text{O}_2/\text{N}_2$ mixtures under
112 pseudo-first-order conditions combined with monitoring of the HCHO reaction products by laser-induced
113 fluorescence (LIF) spectroscopy, and, for the $\text{CH}_2\text{OO} + \text{SO}_2$ reaction at ~1.5 Torr, direct monitoring of
114 CH_2OO by photoionisation mass spectrometry (PIMS). We also report kinetics of the $\text{CH}_2\text{I} + \text{NO}_2$ reaction
115 at pressures between 25 and 300 Torr at 295 K.

116

117 **2. Experimental**

118 **2.1 Laser-Induced Fluorescence Experiments**

119 Apparatus and experimental procedures for the laser-induced fluorescence (LIF) experiments have been
120 described elsewhere in detail,^{26, 32} therefore only a brief description is given here. Kinetics of CH_2OO
121 reactions were studied by monitoring of HCHO reaction products by LIF spectroscopy. Radicals were
122 generated by the laser flash photolysis of $\text{CH}_2\text{I}_2/\text{O}_2/\text{N}_2$ gas mixtures (R1-R2) with the addition of excess co-
123 reagent (NO_2 , NO , SO_2 , H_2O or CH_3CHO) to ensure pseudo-first-order conditions. Experiments to
124 investigate $\text{CH}_2\text{I} + \text{NO}_2$ kinetics were performed in the absence of O_2 , while those to investigate $\text{CH}_2\text{OO} +$
125 NO_2 were performed using a limited range of NO_2 concentrations in order to avoid production of HCHO
126 through the reaction of CH_2I with NO_2 (see Section 3.1), whilst maintaining pseudo-first-order conditions.

127 CH_2I_2 (Sigma-Aldrich, 99 %) was used as a dilute gas in N_2 either by filling a glass bulb containing liquid
128 CH_2I_2 with N_2 or by bubbling a slow flow of N_2 through liquid CH_2I_2 . Reagents (NO , NO_2 , SO_2 , CH_3CHO)
129 were prepared at known concentrations in N_2 and stored in glass bulbs. NO (BOC Special Gases, 99.5 %)
130 was purified prior to use by a series of freeze-pump-thaw cycles. CH_2I_2 , CH_3CHO (Sigma-Aldrich, 99.5

131 %), NO₂ (Sigma-Aldrich, 99.5 %), SO₂ (Sigma-Aldrich, 99.9 %), N₂ (BOC, 99.99 %) and O₂ (BOC, 99.999
132 %) were used as supplied. Water vapour was added to the gas mixture by bubbling a known flow of N₂ gas
133 through a bubbler containing deionised water at a known temperature. Gases were mixed in a gas manifold
134 and passed into a six-way cross reaction cell at known flow rates (determined by calibrated mass flow
135 controllers). The pressure in the reaction cell was monitored by a capacitance manometer (MKS
136 Instruments, 626A) and controlled by throttling the exit valve to the reaction cell. The total gas flow rate
137 through the reaction cell was adjusted with total pressure to maintain an approximately constant gas
138 residence time in the cell (~0.1 s). All experiments were performed at $T = (295 \pm 2)$ K unless stated
139 otherwise.

140 For experiments using NO₂, NO, CH₃CHO or H₂O as co-reagents, initiation of chemistry within the cell
141 was achieved using an excimer laser (KrF, Tui ExciStar M) operating at $\lambda = 248$ nm with typical laser
142 fluence in the range 30 – 80 mJ cm⁻². Experiments in which SO₂ was present as the co-reagent were
143 performed at a photolysis wavelength of 355 nm (typical fluence ~ 150 mJ cm⁻²), generated by frequency
144 tripling the output of a Nd:YAG laser (Spectron Laser Systems) to avoid potential multi-photon photolysis
145 of SO₂ at shorter wavelengths.³³⁻³⁵

146 Production of HCHO was monitored by laser-induced fluorescence (LIF) of HCHO at $\lambda \sim 353.1$ nm.³⁶
147 Approximately 2 to 4 mJ pulse⁻¹ of laser light at ~ 353.1 nm was generated by a dye laser (Lambda Physik,
148 FL3002) operating on DMQ/dioxirane dye and pumped by a 308 nm excimer laser generating ~ 50 mJ
149 pulse⁻¹ (XeCl, Lambda Physik LPX100). The output of the dye laser was passed through the reaction cell
150 in an orthogonal axis to the 248 nm / 355 nm photolysis laser output, with HCHO fluorescence detected in
151 the visible region of the spectrum by a channel photomultiplier (CPM, Perkin-Elmer C1943P) orthogonal to
152 both the photolysis laser and the LIF excitation laser beams. A Perspex filter was used to prevent scattered
153 laser light from the photolysis laser and the LIF excitation laser reaching the CPM. The HCHO
154 fluorescence signal was monitored as a function of time following photolysis of CH₂I₂ by varying the time
155 delay between firing the photolysis laser and the LIF excitation laser through use of a delay generator (SRS
156 DG535). Results from between 5 and 20 photolysis shots were typically averaged prior to analysis.

158 2.2 Photoionisation Mass Spectrometry Experiments

159 Photoionisation mass spectrometry (PIMS) experiments were performed in this work to determine the
160 kinetics of CH₂OO + SO₂ at low pressure (~1.5 Torr) and 295 K by direct monitoring of CH₂OO in
161 reactions performed under pseudo-first-order conditions. The PIMS apparatus has been described
162 previously in detail^{32, 37, 38} and only a brief description is given here. Gas mixtures of CH₂I₂/O₂/N₂ and
163 CH₂I₂/O₂/N₂/SO₂ were prepared in a gas handling line, with reagents and reagent preparation as described
164 above for the LIF experiments, and introduced to the steel reaction flow tube (10.5 mm internal diameter,

165 70 cm in length) *via* calibrated mass flow controllers. The pressure in the reaction flow tube was monitored
166 by a capacitance manometer (MKS Instruments, 626A) and controlled by throttling the exit valve to the
167 flow tube.

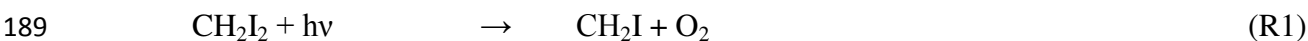
168 Chemistry was initiated by a pulsed excimer laser (Lambda Physik, Compex 205) at a wavelength of 248
169 nm, with typical fluence of $\sim 50 \text{ mJ cm}^{-2}$, through reactions R1 and R2. A representative sample from the
170 reaction mixture effused into a high vacuum chamber ($< 10^{-5}$ Torr, maintained by diffusion and turbo
171 pumps) *via* a 1 mm pinhole situated in the sidewall of the reaction flow tube. Components of the gas
172 mixture were photoionised using 118 nm vacuum ultraviolet (VUV) laser light (typically 10^{11} photons
173 pulse⁻¹), generated by frequency tripling of the third harmonic of a Nd:YAG laser (Continuum Powerlite,
174 8010) in a Xe gas cell, and passed across the effusing gas flow within 2-3 mm of the sampling pinhole.
175 VUV light of 118 nm (equivalent to 10.5 eV) is sufficiently energetic to ionise CH₂OO (threshold = 10.02
176 eV), but is below the threshold required to ionise other isomers at $m/z = 46$ (dioxirane, threshold = 10.82
177 eV; formic acid, threshold = 11.33 eV).¹⁰ Ions were sampled by the time of flight mass spectrometer (TOF-
178 MS, Kore Technology Ltd.), and detected by an electron multiplier. The ion signals were amplified and
179 boxcar averaged on an oscilloscope and then stored on the control computer. The ion signals were
180 monitored as a function of time following photolysis of CH₂I₂ by varying the time delay between the
181 excimer laser and the Nd:YAG laser, used to generate the VUV radiation, through use of a delay generator
182 (SRS DG35). These kinetic traces consisted of typically 200 time points, with typically between 10 and 25
183 shot averaging per time point.

184

185 3. Results and Discussion

186 3.1 Photolysis of CH₂I₂/O₂/N₂ mixtures

187 Figure 1 shows the HCHO fluorescence signal following photolysis of CH₂I₂/O₂/N₂ mixtures (*i.e.* in the
188 absence of any additional co-reagent), resulting in production of HCHO through reactions R1-R6:^{26,32}



196 Previous work in this laboratory²⁶ has shown that the yields of CH₂OO and CH₂IO₂ from R2 are dependent
 197 on pressure, owing to initial formation of the excited species CH₂IO₂[#], which can either decompose to
 198 produce the CH₂OO Criegee intermediate and iodine atoms (R2a) or can be collisionally stabilised to
 199 produce the peroxy radical CH₂IO₂ (R2b). Since subsequent reactions of both CH₂OO and CH₂IO₂ in the
 200 absence of any additional co-reagent result in production of HCHO, there is no change in the total HCHO
 201 yield as a function of pressure following photolysis of CH₂I₂/O₂/N₂ mixtures.

202 Production of HCHO in reactions R1-R6 can be approximated by Equation 1:^{26, 32}

$$203 \quad S_{\text{HCHO},t} = S_0 [\exp(-k_{\text{loss}}t)] + \frac{S_1 k'_g}{k'_g - k_{\text{loss}}} [\exp(-k_{\text{loss}}t) - \exp(-k'_g t)] \quad (\text{Equation 1})$$

204 where $S_{\text{HCHO},t}$ is the HCHO signal at time t , S_0 is the height of the HCHO signal at time zero, S_1 is the
 205 maximum HCHO signal, k'_g is the pseudo-first-order rate coefficient for HCHO growth, and k_{loss} is the rate
 206 coefficient representing the slow loss of HCHO from the detection region *via* diffusion. Although the
 207 HCHO growth through reactions R1-R6 is not strictly first-order, our previous work²⁶ demonstrates that
 208 Equation 1 can faithfully reproduce the HCHO growth kinetics. In the presence of excess co-reagent (*e.g.*
 209 SO₂, NO₂) the kinetics of HCHO production from CH₂OO are under pseudo-first-order conditions. Figure
 210 1 shows the fits to HCHO production in the absence and presence of additional co-reagent, indicating the
 211 fidelity of the fit to the analytical equation.

212 In the absence of any additional co-reagent, the first-order rate coefficient approximating the production of
 213 HCHO, k'_g , was found to vary from ~300 s⁻¹ to ~3500 s⁻¹, depending on the concentration of CH₂I₂, and
 214 thus of I atoms, in the system, in keeping with the work of Welz *et al.*¹⁰ and Taatjes *et al.*¹¹ Some initial
 215 HCHO production was observed owing to multi-photon photolysis of CH₂I₂ and the subsequent rapid
 216 reaction of ³CH₂ with O₂, with S_0 typically no greater than 5 – 10 % of S_1 .³⁹⁻⁴³

217

218 **3.2 CH₂OO + SO₂**

219 The reaction of CH₂OO with SO₂ (R7) was investigated in separate experiments using the PIMS method to
 220 monitor CH₂OO and the LIF method to monitor HCHO production.



222 Experiments using the PIMS method were performed at a total pressure of 1.5 Torr. Figure 2 shows a
 223 typical decay for CH₂OO observed in the presence of excess SO₂, with the pseudo-first-order rate
 224 coefficient for CH₂OO decay found by least-squares fitting to Equation 2:

$$S_{\text{CH}_2\text{OO},t} = \frac{S_{\text{max}} k_{\text{sampling}}}{k_{\text{sampling}} - k'} \left[\exp(-k' t) - \exp(-k_{\text{sampling}} t) \right] \quad (\text{Equation 2})$$

where $S_{\text{CH}_2\text{OO},t}$ is the CH_2OO ion signal at time t , S_{max} is the maximum CH_2OO ion signal, k' is the pseudo-first-order rate coefficient for CH_2OO decay, and k_{sampling} is the rate coefficient representing the transport of molecules in the reactor to the ionisation region ($\sim 30,000 \text{ s}^{-1}$, described in detail by Baeza-Romero *et al.*³⁸).

The bimolecular rate coefficient for $\text{CH}_2\text{OO} + \text{SO}_2$ (k_7) determined using the PIMS method at 1.5 Torr was $(3.6 \pm 0.5) \times 10^{-11} \text{ cm}^3 \text{ s}^{-1}$ (Figure 3), similar to the value of $(3.9 \pm 0.7) \times 10^{-11} \text{ cm}^3 \text{ s}^{-1}$ at 4 Torr reported by Welz *et al.*¹⁰ and several orders of magnitude greater than the values typically used in atmospheric models.

The LIF experiments monitoring HCHO production from $\text{CH}_2\text{OO} + \text{SO}_2$ were performed over the pressure range 50 – 450 Torr, with SO_2 concentrations in the range 2.4×10^{14} to $1.6 \times 10^{15} \text{ cm}^{-3}$. The HCHO growth (Figure 4) was observed to display biexponential behaviour, with no decrease in the total HCHO yield compared to experiments performed in the absence of any co-reagent, indicating complete titration of both CH_2OO and CH_2IO_2 to HCHO. Kinetic parameters were determined by fitting to Equation 3:

$$S_{\text{HCHO},t} = S_0 \left[\exp(-k_{\text{loss}} t) \right] + \frac{S_1 f k'_{g1}}{k'_{g1} - k_{\text{loss}}} \left[\exp(-k_{\text{loss}} t) - \exp(-k'_{g1} t) \right] + \frac{S_1 (1-f) k'_{g2}}{k'_{g2} - k_{\text{loss}}} \left[\exp(-k_{\text{loss}} t) - \exp(-k'_{g2} t) \right] \quad (\text{Equation 3})$$

where $S_{\text{HCHO},t}$ is the HCHO signal at time t , S_0 is the height of the HCHO signal at time zero, S_1 is the maximum HCHO signal, k'_{g1} is the pseudo-first-order rate coefficient for the fast HCHO growth, k'_{g2} is the pseudo-first-order rate coefficient for the slower HCHO growth, f is the fractional contribution of the fast growth process to the total HCHO yield (hence $(1-f)$ is the fractional contribution of the slower growth process to the total HCHO yield), and k_{loss} is the rate coefficient representing the slow loss of HCHO from the detection region *via* diffusion. For the SO_2 experiments (conducted using a photolysis wavelength of 355 nm) there was no contribution from S_0 (*i.e.* $S_0 = 0$).

The initial fast growth of HCHO displayed a linear dependence on $[\text{SO}_2]$, while the slower growth was independent of $[\text{SO}_2]$ and at a similar rate to the observed HCHO production in the absence of any additional co-reagent. The yields of HCHO from the faster growth process were consistent with production from $\text{CH}_2\text{OO} + \text{SO}_2$, while those from the slower process were consistent with production from reactions of CH_2IO_2 (*i.e.* reactions R4-R6). We thus determine k_7 from linear fits of k'_{g1} (Equation 3) against $[\text{SO}_2]$. The validity of describing the system using Equation 3 is discussed in our previous work.²⁶

Figure 5 and Table 1 show the values of k_7 as a function of pressure. No significant dependence of k_7 on pressure was observed, with an average value of $(3.42 \pm 0.42) \times 10^{-11} \text{ cm}^3 \text{ s}^{-1}$ for all experiments (PIMS and LIF) described in this work (all errors are 1σ unless stated otherwise). Moreover, there is no significant change in the HCHO yield from the reaction of CH_2OO with SO_2 as a function of pressure, indicating there is little stabilisation of reaction products. These results are consistent with the low pressure results obtained by Welz *et al.*¹⁰ and theoretical work by Vereecken *et al.*¹³, and support arguments for an increased role of $\text{CH}_2\text{OO} + \text{SO}_2$ in the atmosphere. Taatjes *et al.*¹² have also shown that the reaction of the C_2 Criegee intermediate, CH_3CHOO , with SO_2 at a pressure of 4 Torr is also significantly faster than previously expected, potentially indicating an increased role for $\text{CH}_3\text{CHOO} + \text{SO}_2$ in the atmosphere. However, theoretical calculations predict that reactions of larger Criegee intermediates will exhibit pressure dependence,¹³ and that production of SO_3 in reactions of larger Criegee intermediates at atmospheric pressures is unlikely owing to stabilisation of SO_2 -Criegee intermediate complexes to produce secondary ozonide species, thus reducing the impacts of $\text{SO}_2 + \text{Criegee}$ intermediate reactions on H_2SO_4 and sulfate aerosol production.¹³ Field observations and laboratory studies by Mauldin *et al.*²³ indicate that larger Criegee intermediates, such as those produced in the ozonolysis of monoterpenes, do impact on atmospheric concentrations of H_2SO_4 through oxidation of SO_2 , but that the impacts may not be as great as those reported for CH_2OO , potentially owing to stabilisation of reaction products. Further work is thus required to investigate the effects of pressure on the reactions of larger Criegee intermediates. Moreover, modelled impacts of increases in the rates of Criegee intermediate reactions with SO_2 are highly dependent on the competition with rates of Criegee intermediate reactions with water vapour. We thus investigate $\text{CH}_2\text{OO} + \text{H}_2\text{O}$ in Section 3.6.

3.3 $\text{CH}_2\text{I} + \text{NO}_2$

Production of HCHO following photolysis of $\text{CH}_2\text{I}_2/\text{NO}_2/\text{N}_2$ mixtures was examined as a function of pressure to facilitate assessment of the competition between $\text{CH}_2\text{I} + \text{O}_2$ (R2) and $\text{CH}_2\text{I} + \text{NO}_2$ (R8) in $\text{CH}_2\text{OO} + \text{NO}_2$ experiments (Section 3.4).



The production of HCHO could be described by Equation 1 (above), where $k'_g = k_8[\text{NO}_2]$, with concentrations of NO_2 between 1×10^{14} and $9 \times 10^{14} \text{ cm}^{-3}$. Pseudo-first-order rate coefficients (k'_g) were in the range ~ 5000 to $45,000 \text{ s}^{-1}$, and typically large compared to the rate coefficients describing HCHO production in the absence of any additional co-reagent (Section 3.1). The bimolecular rate coefficient k_8 was determined from plots of k'_g against $[\text{NO}_2]$ at each pressure (Figure S1), and was found to increase with increasing pressure (Figure S2 and Table S1), with a corresponding decrease in the HCHO yield as the pressure was increased (Figure S3).

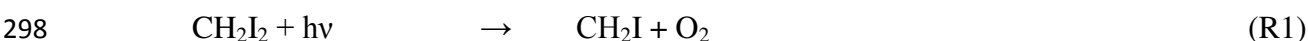
285 A previous investigation of $\text{CH}_2\text{I} + \text{NO}_2$ at pressures of 2 to 5 Torr gave a value of $k_8 = (2.2 \pm 0.1) \times 10^{-11}$
286 $\text{cm}^3 \text{s}^{-1}$.⁴⁴ Results of this work show k_8 to be $(2.56 \pm 0.17) \times 10^{-11} \text{cm}^3 \text{s}^{-1}$ at 50 Torr, increasing to $(5.07 \pm$
287 $0.28) \times 10^{-11} \text{cm}^3 \text{s}^{-1}$ at 300 Torr.

288 The rate coefficient for reaction of CH_2I radicals with O_2 (R2), has been shown previously to be $\sim 1.6 \times 10^{-12}$
289 $\text{cm}^3 \text{s}^{-1}$.^{45, 46} Experiments to investigate HCHO production in the reaction of CH_2OO (produced by CH_2I
290 + O_2) with NO_2 must therefore be conducted at sufficiently high $[\text{O}_2]$ to avoid complications owing to
291 HCHO production from $\text{CH}_2\text{I} + \text{NO}_2$.

292

293 3.4 $\text{CH}_2\text{OO} + \text{NO}_2$

294 Experiments to investigate $\text{CH}_2\text{OO} + \text{NO}_2$ (R9) kinetics were performed with sufficient NO_2 concentrations
295 (1.0×10^{14} to $1.4 \times 10^{15} \text{cm}^{-3}$) to ensure pseudo-first-order conditions for CH_2OO loss whilst also ensuring
296 that $k_2[\text{O}_2] > k_8[\text{NO}_2]$ at all times to avoid potential complications owing to HCHO production through
297 $\text{CH}_2\text{I} + \text{NO}_2$.



302 Figure 1 shows the evolution of the HCHO signal following photolysis of $\text{CH}_2\text{I}_2/\text{O}_2/\text{N}_2/\text{NO}_2$ mixtures.
303 Experiments in which NO_2 was used as a co-reagent resulted in a decrease in the total HCHO yield when
304 compared to experiments performed in the absence of any co-reagent. We attribute this to the formation of
305 the peroxy nitrate species $\text{CH}_2\text{IO}_2\text{NO}_2$ which inhibits formation of HCHO through reactions R4-R6.

306 Experiments performed at 273 K to increase the lifetime of $\text{CH}_2\text{IO}_2\text{NO}_2$ with respect to dissociation to
307 $\text{CH}_2\text{IO}_2\text{NO}_2$ did not result in any significant decrease in the HCHO yield compared to equivalent
308 experiments at 295 K, indicating that the $\text{CH}_2\text{IO}_2\text{NO}_2$ lifetime at 295 K is sufficiently long to minimise
309 production of HCHO from CH_2IO_2 . Thus, while there is a small contribution to the HCHO signal owing to
310 rapid chemistry following multi-photon photolysis of CH_2I_2 , the growth of HCHO observed following
311 photolysis of $\text{CH}_2\text{I}_2/\text{O}_2/\text{N}_2/\text{NO}_2$ mixtures can be attributed to $\text{CH}_2\text{OO} + \text{NO}_2$ (R9) exclusively.

312 The pseudo-first-order rate coefficient for the reaction of CH_2OO with NO_2 was determined by least-
313 squares fitting to Equation 1, with $k'_g = k_9[\text{NO}_2]$. The bimolecular rate coefficient for $\text{CH}_2\text{OO} + \text{NO}_2$ (k_9)
314 was subsequently determined from plots of k'_g against $[\text{NO}_2]$, as shown in Figure 6. Fits to experimental

315 data using the numerical integration package Kintecus⁴⁷ to determine k_9 , detailed in the supplementary
316 information, gave results within 10 % of those obtained using the analytical expression (Equation 1).

317 Values for k_9 as a function of pressure are shown in Figure 7 and Table 2. No significant dependence of k_9
318 on total pressure was observed over the pressure range investigated (25 to 300 Torr), with an average value
319 of $k_9 = (1.5 \pm 0.5) \times 10^{-12} \text{ cm}^3 \text{ s}^{-1}$. Errors in k_9 include the 1σ errors in the fits to the bimolecular plots at
320 each pressure and an error of $\pm 10 \%$ to account for any differences between fits using the analytical
321 expression and those obtained by numerical integration (see supplementary information).

322 Yields of HCHO in the presence of NO_2 , determined relative to experiments performed in the absence of
323 NO_2 (*i.e.* production through reactions R3-R6), were consistent with the yields of CH_2OO determined in
324 our previous work²⁶ (Figure 8). This result demonstrates that $\sim 100 \%$ of CH_2OO is titrated to HCHO by
325 $\text{CH}_2\text{OO} + \text{NO}_2$, indicating a lack of pressure dependence in k_9 , and that there is insignificant HCHO
326 production from CH_2IO_2 in the presence of NO_2 . Recent measurements by Ouyang *et al.*²¹ have
327 demonstrated the production of NO_3 at atmospheric pressure from the reaction of CH_2OO with NO_2 , thus
328 also suggesting little stabilisation of reaction products to a secondary ozonide species in this system.

329 No significant difference in k_9 or in yields of HCHO were observed between experiments performed in O_2
330 bath gas and N_2 bath gas (results shown in Table 2), providing further evidence for similar quenching of the
331 nascent excited $\text{CH}_2\text{IO}_2^\#$ species (produced in R2) by O_2 and N_2 , as discussed in our previous work.²⁶

332 Results for k_9 obtained in this work, while lower than those reported by Welz *et al.*¹⁰, are on the same order
333 of magnitude, and demonstrate a significantly faster reaction between CH_2OO and NO_2 than suggested by
334 previous indirect measurements.¹

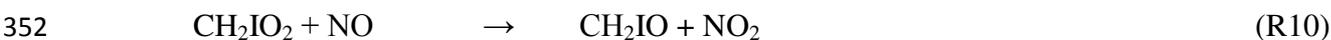
335

336 3.5 $\text{CH}_2\text{OO} + \text{NO}$

337 Production of HCHO following photolysis of $\text{CH}_2\text{I}_2/\text{O}_2/\text{N}_2$ mixtures in the presence of excess NO ($3.6 \times$
338 10^{14} to $1.7 \times 10^{15} \text{ cm}^{-3}$) exhibits biexponential growth, as shown in Figure 9, similar to experiments with
339 SO_2 . Again, no decrease in the total HCHO yield compared to experiments performed in the absence of
340 any co-reagent, indicating complete titration of both CH_2OO and CH_2IO_2 to HCHO. Kinetic parameters for
341 the processes contributing to HCHO production were obtained by fitting to Equation 3 (above).

342 The rate coefficient describing the fast HCHO growth process, k'_{g1} , was observed to increase linearly with
343 increasing $[\text{NO}]$, with the slope of a plot of k'_{g1} against $[\text{NO}]$ giving a bimolecular rate coefficient of $(1.07 \pm$
344 $0.06) \times 10^{-11} \text{ cm}^3 \text{ s}^{-1}$ at 250 Torr (Figure S4). The rate coefficient describing the slower HCHO growth, k'_{g2} ,
345 was found to be independent of $[\text{NO}]$, and similar to the rate coefficient for HCHO production obtained in
346 the absence of NO. Reactions of peroxy radicals (RO_2) with NO are well established, and are typically on
347 the order of 10^{-12} to $10^{-11} \text{ cm}^3 \text{ s}^{-1}$,^{48,49} with a rate coefficient for $\text{CH}_3\text{O}_2 + \text{NO}$ of $7.2 \times 10^{-12} \text{ cm}^3 \text{ s}^{-1}$,⁴⁹ while

348 Welz *et al.*¹⁰ reported an upper limit of $6 \times 10^{-14} \text{ cm}^3 \text{ s}^{-1}$ for the rate coefficient for CH_2OO with NO . Thus,
349 in contrast to the experiments with SO_2 , we attribute the fast HCHO growth to the rapid decomposition of
350 CH_2IO (R6), produced in the reaction of CH_2IO_2 with NO (R10) and assign $k_{10} = (1.07 \pm 0.06) \times 10^{-11}$
351 $\text{cm}^3 \text{ s}^{-1}$ at 250 Torr.



354 The slower HCHO growth thus contains contributions from $\text{CH}_2\text{OO} + \text{I}$ (R3) and potentially $\text{CH}_2\text{OO} + \text{NO}$
355 (R11). In the absence of NO , production of HCHO was observed with a pseudo-first-order rate coefficient
356 of $1860 \pm 100 \text{ s}^{-1}$ (Equation 1). On addition of up to $1.7 \times 10^{15} \text{ cm}^{-3}$ NO , the average value for the rate
357 coefficient describing the slow HCHO growth (k_{g2} in Equation 3) was $1800 \pm 340 \text{ s}^{-1}$. Any potential
358 influence of NO on the observed rates of HCHO production is assumed to be within the error of the
359 experiment, and we thus place an upper limit of $2 \times 10^{-13} \text{ cm}^3 \text{ s}^{-1}$ on the rate coefficient for reaction of
360 $\text{CH}_2\text{OO} + \text{NO}$ (k_{11}).



362 The upper limit for k_{11} determined here is higher than that reported by Welz *et al.* ($k_{11} < 6 \times 10^{-14} \text{ cm}^3 \text{ s}^{-1}$),
363 owing to increased uncertainties associated with the biexponential fit, relatively low concentrations of NO ,
364 and higher concentrations of CH_2I_2 used in these experiments compared to those performed by Welz *et al.*,
365 which lead to increased iodine atom concentrations in this work and thus increased rates of HCHO
366 production through $\text{CH}_2\text{OO} + \text{I}$ (R3). In subsequent experiments (notably those used to investigate the
367 kinetics of $\text{CH}_2\text{OO} + \text{H}_2\text{O}$) lower CH_2I_2 concentrations were used by changing the delivery method for
368 CH_2I_2 . There are also additional uncertainties in the rate coefficients for reactions with NO owing to the
369 potential for production of NO_2 in the gas lines leading to the reaction cell through oxidation of NO by O_2
370 (the gas mixture has a residence time of $\sim 1 \text{ s}$ in the gas lines leading from the mixing line to the reaction
371 cell), leading to the potential for contributions to the observed HCHO growth from reactions involving
372 NO_2 .

373

374 **3.6 $\text{CH}_2\text{OO} + \text{H}_2\text{O}$**

375 Welz *et al.* did not observe any change in the rate of CH_2OO decay on addition of water vapour to the
376 system, and reported an upper limit of $4 \times 10^{-15} \text{ cm}^3 \text{ s}^{-1}$ for the rate coefficient for reaction of CH_2OO with
377 H_2O (R12):



379 Similarly to the results of Welz *et al.*, the addition of water vapour to the LIF experiments in this work did
380 not result in any significant change to the rate of HCHO production. The total HCHO yield was also
381 unaffected by the presence of water vapour, indicating complete titration of CH₂OO and CH₂IO₂ to HCHO
382 through reactions R3-R6. Figure 10 shows the HCHO fluorescence signals following photolysis of
383 CH₂I₂/O₂/N₂ in the absence and presence of water vapour. While the HCHO signal is reduced in the
384 presence of water vapour, there is no change in the kinetics and the reduction in signal is attributed to
385 increased fluorescence quenching by water vapour.

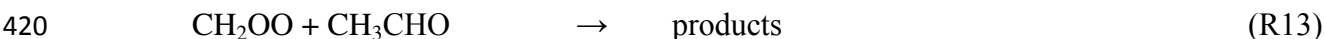
386 At 200 Torr the pseudo-first-order rate coefficient for HCHO production was determined to be $41 \pm 15 \text{ s}^{-1}$
387 by fitting to Equation 1, and was lower than the typical values reported in Section 3.1 as a result of lower
388 concentrations of CH₂I₂ to reduce the rate of HCHO production through radical-radical reactions in the
389 absence of water vapour. On addition of up to $1.7 \times 10^{17} \text{ cm}^{-3}$ water vapour to the system, a value of $52 \pm$
390 13 s^{-1} was obtained, with no obvious dependence on the concentration of water vapour added. Owing to the
391 higher total pressures used in this work, enabling the addition of a higher number density of water vapour to
392 the system compared to the low pressure experiments by Welz *et al.*, we are able to place an upper limit of
393 $9 \times 10^{-17} \text{ cm}^3 \text{ s}^{-1}$ on k_{12} at 295 K by assuming any influence of water vapour is within the error of the
394 experiment. Ouyang *et al.*²¹ have reported a value for k_{12} of $(2.5 \pm 1) \times 10^{-17} \text{ cm}^3 \text{ s}^{-1}$ at 760 Torr,
395 determined in a relative rate experiment monitoring NO₃ production and using the absolute value for k_9
396 (CH₂OO + NO₂) reported by Welz *et al.*¹⁰ ($7 \times 10^{-12} \text{ cm}^3 \text{ s}^{-1}$). Using the relative rate coefficient ratio
397 reported by Ouyang *et al.*, with the value for k_9 determined in this work ($1.5 \times 10^{-12} \text{ cm}^3 \text{ s}^{-1}$), a value of k_{12}
398 $= 5.4 \times 10^{-18} \text{ cm}^3 \text{ s}^{-1}$ can be obtained.

399 Modelling studies investigating the impacts of CH₂OO chemistry on the atmospheric oxidation of SO₂ may
400 therefore be underestimating the effects of increasing the rate coefficient for CH₂OO + SO₂ owing to
401 overestimation of the competition with CH₂OO + H₂O, resulting in more significant impacts on
402 atmospheric production of H₂SO₄ and sulfate aerosol than indicated thus far. However, Taatjes *et al.*¹² have
403 shown that the *anti*-CH₃CHOO Criegee intermediate does react with water vapour ($k = (1.0 \pm 0.4) \times 10^{-14}$
404 $\text{cm}^3 \text{ s}^{-1}$), and the lack of reaction between CH₂OO and water vapour may not be representative of all
405 Criegee intermediates. Modelling of Criegee chemistry in forested regions in Finland and Germany has
406 indicated that concentration of the CH₂OO Criegee intermediate is only ~20-33 % of the concentrations of
407 larger Criegee intermediates derived from monoterpenes,¹⁴ with global modelling indicating that the
408 production rate of CH₂OO comprises ~40 % of the total global production rate of all Criegee
409 intermediates.¹⁵ The chemistry of larger Criegee intermediates warrants further attention.

411 3.7 CH₂OO + CH₃CHO

412 The reactions of Criegee intermediates with carbonyl compounds are of interest not only for their potential
413 atmospheric relevance, but also to facilitate the use of carbonyl compounds as scavengers of Criegee
414 intermediates in alkene ozonolysis experiments, enabling the determination of product yields of ozonolysis
415 reactions.

416 Horie *et al.*⁵⁰ studied the relative rates of CH₂OO reactions with CH₃CHO (R13) and CF₃COCF₃ (R14) at
417 730 Torr in synthetic air using FT-IR spectroscopy to monitor the decay of CF₃COCF₃ and the production
418 of the secondary ozonide propene ozonide (methyl-1,2,4-trioxolane) from the reaction with CH₃CHO, and
419 found the reaction with CF₃COCF₃ to be 13 times faster than that with CH₃CHO.

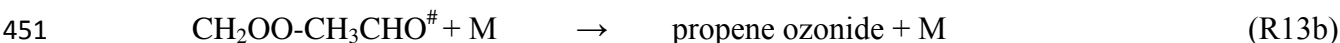
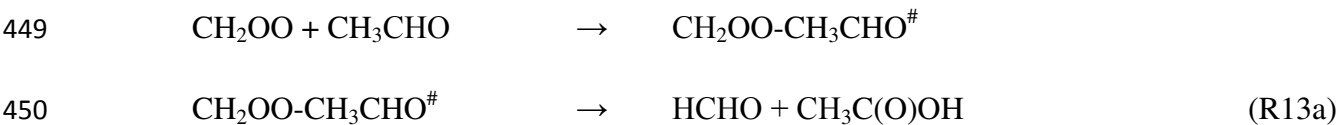


422 Secondary ozonide products were observed by Horie *et al.* for both R13 and R14 at 730 Torr, while
423 photoionisation mass spectrometry experiments by Taatjes *et al.*¹¹ at 4 Torr observed a secondary ozonide
424 product for R14 but not for R13. Absolute rate coefficients for CH₂OO + CH₃CHO and CH₂OO +
425 CF₃COCF₃ were measured by Taatjes *et al.*¹¹ at 4 Torr in He by direct monitoring of CH₂OO, with results
426 indicating the reaction with CF₃COCF₃ to be ~32 times faster than that with CH₃CHO and $k_{13} = (9.4 \pm 0.7)$
427 $\times 10^{-13} \text{ cm}^3 \text{ s}^{-1}$ at 4 Torr. As discussed by Taatjes *et al.*¹¹, the differences between the results of Horie *et al.*
428 and Taatjes *et al.* may arise from differences in the fall-off behaviour of the two reactions, indicating
429 pressure dependence of one or both of the reactions over the range of pressures investigated. Differences in
430 product observations between the two studies also suggest pressure dependence in k_{13} . In the low pressure
431 experiments, Taatjes *et al.* do not observe formation of secondary ozonide products. At 730 Torr, propene
432 ozonide was observed as the major product of R13, indicating collisional stabilisation of the nascent
433 secondary ozonide at high pressures. Recent theoretical work²² has investigated the potential energy
434 surface for the reaction of CH₂OO with CH₃CHO, and supports the observed pressure dependence of the
435 reaction. Reaction products are predicted to be collisionally stabilised to a secondary ozonide (SOZ)
436 species, with significant production of the SOZ at atmospheric pressure (760 Torr) and the SOZ dominating
437 the reaction products at pressures above 1000 Torr.

438 Pressure dependent kinetics are expected to be typical for reactions of larger Criegee intermediates with
439 atmospherically relevant species, including SO₂, and investigation of the CH₂OO + CH₃CHO system may
440 therefore provide insight to the behaviour of other Criegee intermediates.

441 In this work, we investigate HCHO production from CH₂OO + CH₃CHO (R13) at total pressures between
442 25 and 300 Torr and concentrations of CH₃CHO in the range 2×10^{14} to $1 \times 10^{15} \text{ cm}^{-3}$. Production of
443 HCHO displayed single exponential growth, and the HCHO fluorescence signal was fitted to Equation 1
444 (Figure 11). Figure 12 shows the bimolecular plot used to determine k_{13} at 25 Torr, giving $k_{13} = (1.48 \pm$
445 $0.04) \times 10^{-12} \text{ cm}^3 \text{ s}^{-1}$ at 25 Torr. The HCHO yield from R13 (corrected for any HCHO production from

446 CH₂IO₂ in reactions R4-R6 using the results of our previous work) was observed to decrease with
447 increasing pressure, indicating stabilisation of the CH₂OO + CH₃CHO reaction product at higher pressures
448 (R13b) and pressure dependence in k_{13} .



452 Figure 13 shows the Stern-Volmer plot for HCHO yields from R13, giving an intercept of 1.19 ± 0.39 and
453 slope (k_{13b}/k_{13a}) of $(1.09 \pm 0.08) \times 10^{-18} \text{ cm}^3$. Using an intercept of 1, at 4 Torr we estimate a yield of
454 HCHO of 88 %, with a yield of 4 % at 730 Torr, reconciling the results of Taatjes *et al.*¹¹ and Horie *et al.*⁵⁰
455 and in agreement with theoretical work of Jalan *et al.*²²

456 Owing to the decrease in HCHO yield with increasing pressure, assignment of the kinetics of R13 at
457 pressures above 25 Torr is challenging. Using the results of Taatjes *et al.*¹¹ at 4 Torr ($k_{13} = (9.5 \pm 0.7) \times 10^{-13} \text{ cm}^3 \text{ s}^{-1}$),
458 together with those determined here at 25 Torr ($k_{13} = (1.48 \pm 0.04) \times 10^{-12} \text{ cm}^3 \text{ s}^{-1}$), 50 Torr
459 ($\sim 2.2 \times 10^{-12} \text{ cm}^3 \text{ s}^{-1}$) and the determination of k_{13b}/k_{13a} from the Stern-Volmer plot ($(1.09 \pm 0.08) \times 10^{-18} \text{ cm}^3$),
460 we estimate a low pressure limit ($k_{13,0}$) of $\sim 1.6 \times 10^{-29} \text{ cm}^6 \text{ s}^{-1}$ and a high pressure limit ($k_{13,\text{inf}}$) of \sim
461 $1.7 \times 10^{-12} \text{ cm}^3 \text{ s}^{-1}$ (see supplementary information).

462

463 Conclusions

464 Reactions of the CH₂OO Criegee intermediate with NO₂, NO, SO₂, H₂O and CH₃CHO have been
465 investigated over a range of pressures. The reactions of CH₂OO with NO₂, SO₂ and CH₃CHO are rapid, in
466 agreement with recent measurements by Welz *et al.*¹⁰ and Taatjes *et al.*¹¹ but in contrast to
467 recommendations for atmospheric modelling based on indirect measurements. Rate coefficients for
468 reactions of CH₂OO with NO₂ and SO₂ are essentially independent of pressure over the pressure ranges
469 studied in this work. The rate coefficient for CH₂OO + CH₃CHO is pressure dependent, with stabilisation
470 to form the secondary ozonide reaction products at high pressures.

471 We observe no evidence for reactions of CH₂OO with NO or H₂O under the conditions employed in this
472 work, and place upper limits on rate coefficients for these reactions of $2 \times 10^{-13} \text{ cm}^3 \text{ s}^{-1}$ and $9 \times 10^{-17} \text{ cm}^3 \text{ s}^{-1}$,
473 respectively. The upper limit for the rate coefficient for CH₂OO + H₂O is significantly lower than has
474 been reported previously. Earlier assessments^{2, 14, 15, 17} of the impacts of increased reaction rates for CH₂OO
475 + SO₂ and CH₂OO + NO₂ will therefore be lower limits owing to overestimation of the impacts of CH₂OO
476 + H₂O.

477

478 **Acknowledgements**

479 The authors are grateful to the National Centre for Atmospheric Science (NCAS) and the Engineering and
480 Physical Sciences Research Council (EPSRC, grant reference EP/J010871/1) for funding.

481

Pressure / Torr	$k_7 / 10^{-11} \text{ cm}^3 \text{ s}^{-1}$	Reference
1.5 ^a	3.6 ± 0.5	This work
4	3.9 ± 0.7	Welz <i>et al.</i> ¹⁰
50	3.04 ± 0.66	This work
100	3.11 ± 0.57	This work
150	3.17 ± 0.34	This work
250	3.68 ± 0.21	This work
350	3.19 ± 0.53	This work
450	4.18 ± 0.30	This work

483 Table 1: Bimolecular rate coefficients for $\text{CH}_2\text{OO} + \text{SO}_2$ (k_7) as a function of pressure. Errors are 1σ .484 ^aData at 1.5 Torr are from the PIMS experiments.

485

Pressure / Torr	$k_9 / 10^{-12} \text{ cm}^3 \text{ s}^{-1}$	Reference
4	7_{-2}^{+3}	Welz <i>et al.</i> ¹⁰
25 ^a	1.70 ± 0.38	This work
50 ^a	1.04 ± 0.27	This work
50 ^b	0.94 ± 0.16	This work
75 ^a	1.69 ± 0.28	This work
100 ^a	1.38 ± 0.33	This work
150 ^a	1.19 ± 0.30	This work
200 ^a	2.00 ± 0.56	This work
250 ^a	0.96 ± 0.29	This work
300 ^a	2.53 ± 0.47	This work

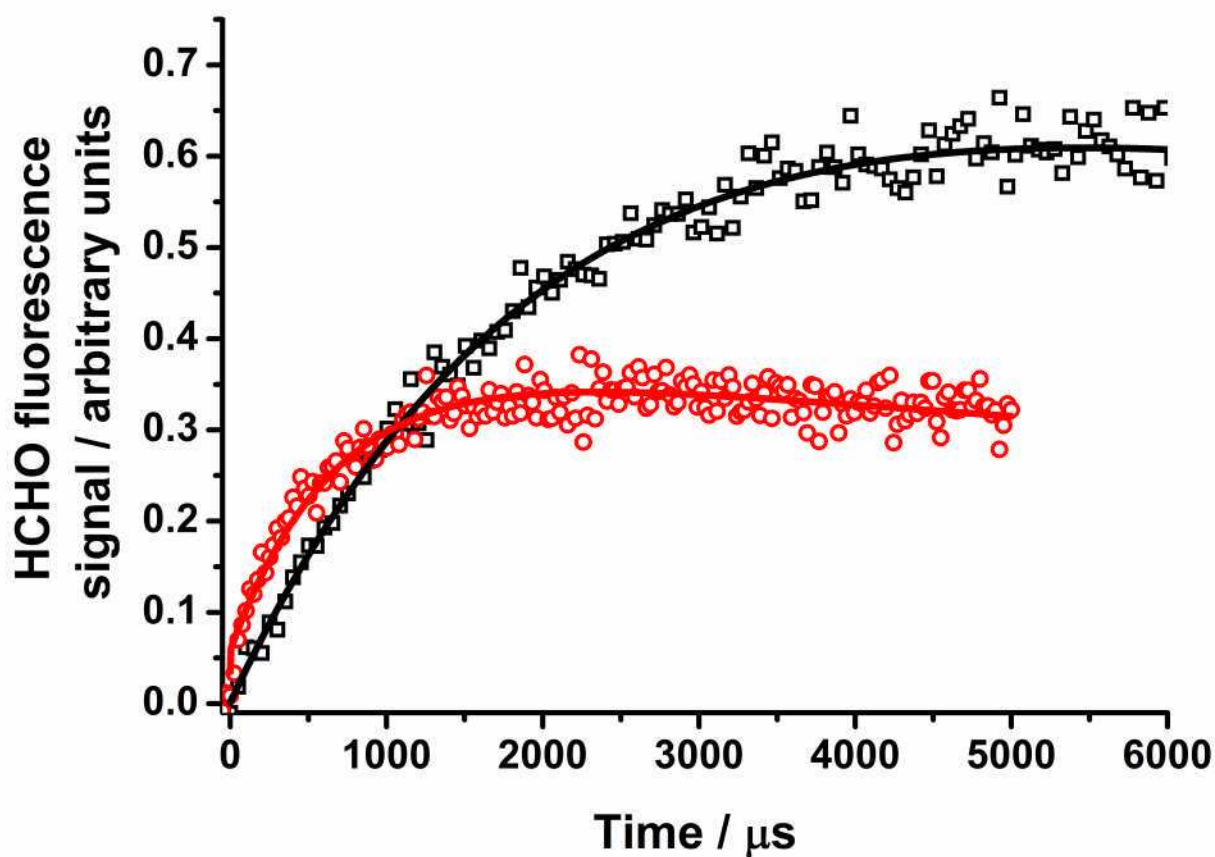
486 Table 2: Bimolecular rate coefficients for $\text{CH}_2\text{OO} + \text{NO}_2$ (k_9) as a function of pressure. Errors include the
487 1σ in the fits to the bimolecular plots and an error of $\pm 10\%$ to account for any differences between the fits
488 using the analytical expression and those obtained by numerical integration. ^aMeasured using N_2 as the
489 bath gas; ^bMeasured using O_2 as the bath gas.

490

491

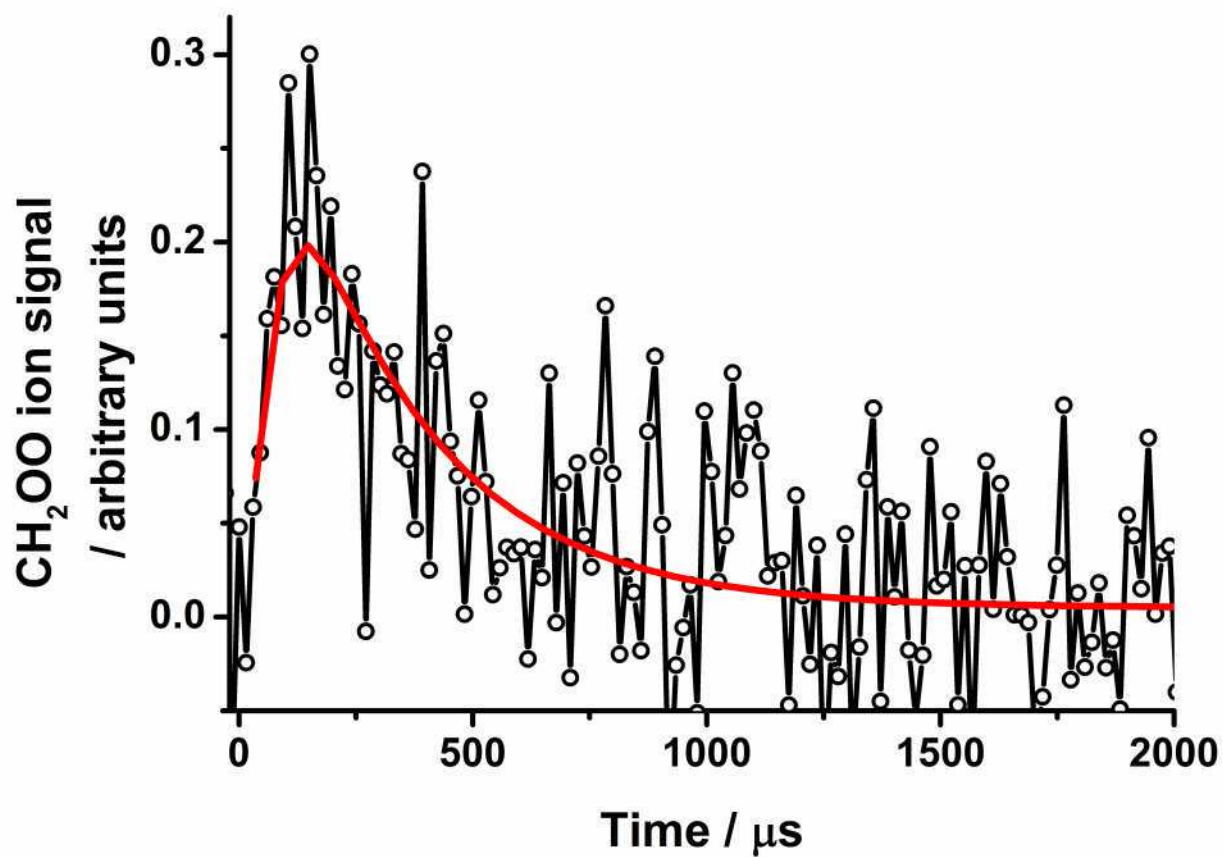
492

493

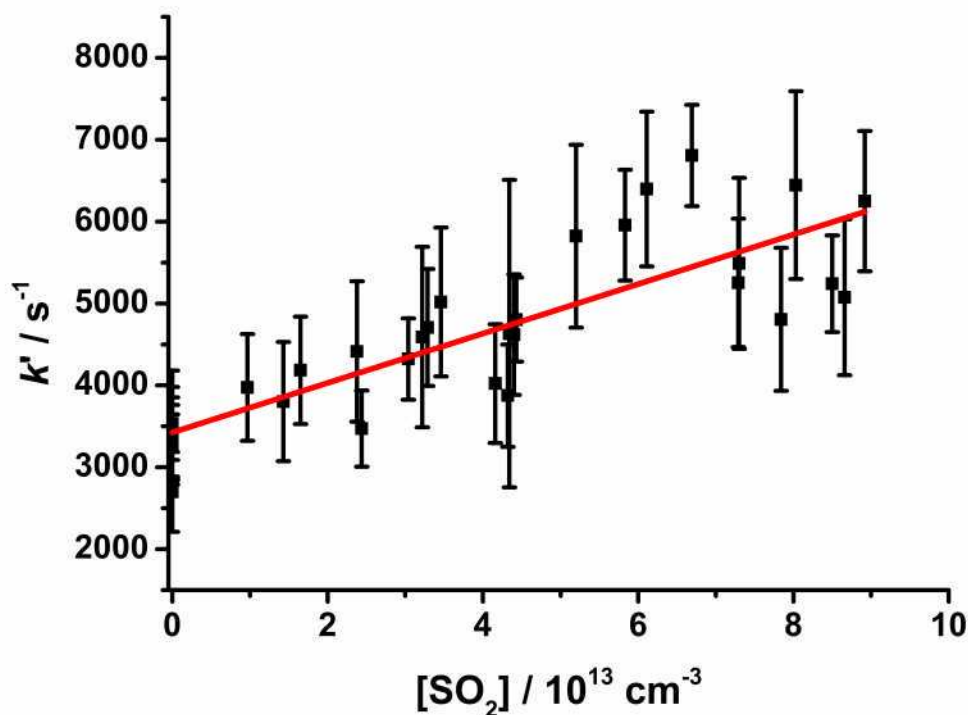


495

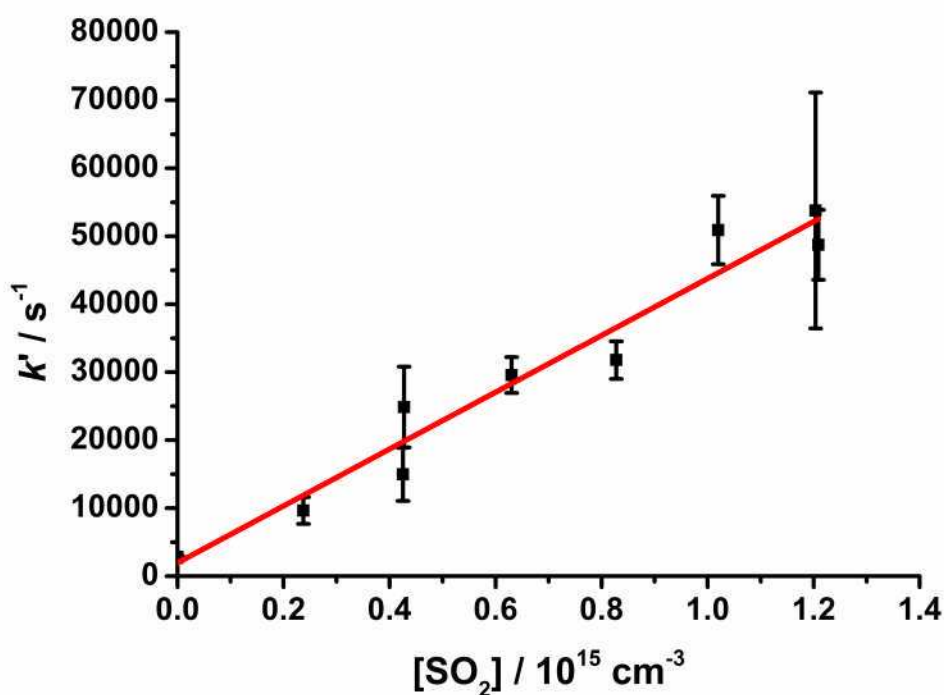
496 Figure 1: HCHO fluorescence signals at 200 Torr following photolysis of CH_2I_2 in the presence of O_2 in the
497 absence of any co-reagent (black open squares) and in the presence of NO_2 (red open circles). The fits to
498 Equation 1 are shown by the solid lines, and give $k'_g = (460 \pm 30) \text{ s}^{-1}$ in the absence of any additional co-
499 reagent and $k'_g = (1490 \pm 50) \text{ s}^{-1}$ in the presence of NO_2 . The ratio of S_1 (Equation 1) in the presence of
500 NO_2 to that in the absence of NO_2 is 0.37.



501 Figure 2: CH₂OO ion signals at 1.5 Torr following photolysis of CH₂I₂/O₂/N₂ in the presence of SO₂, with
502 the fit to Equation 3 (solid red line). For these data, $k' = (3310 \pm 450) \text{ s}^{-1}$.
503

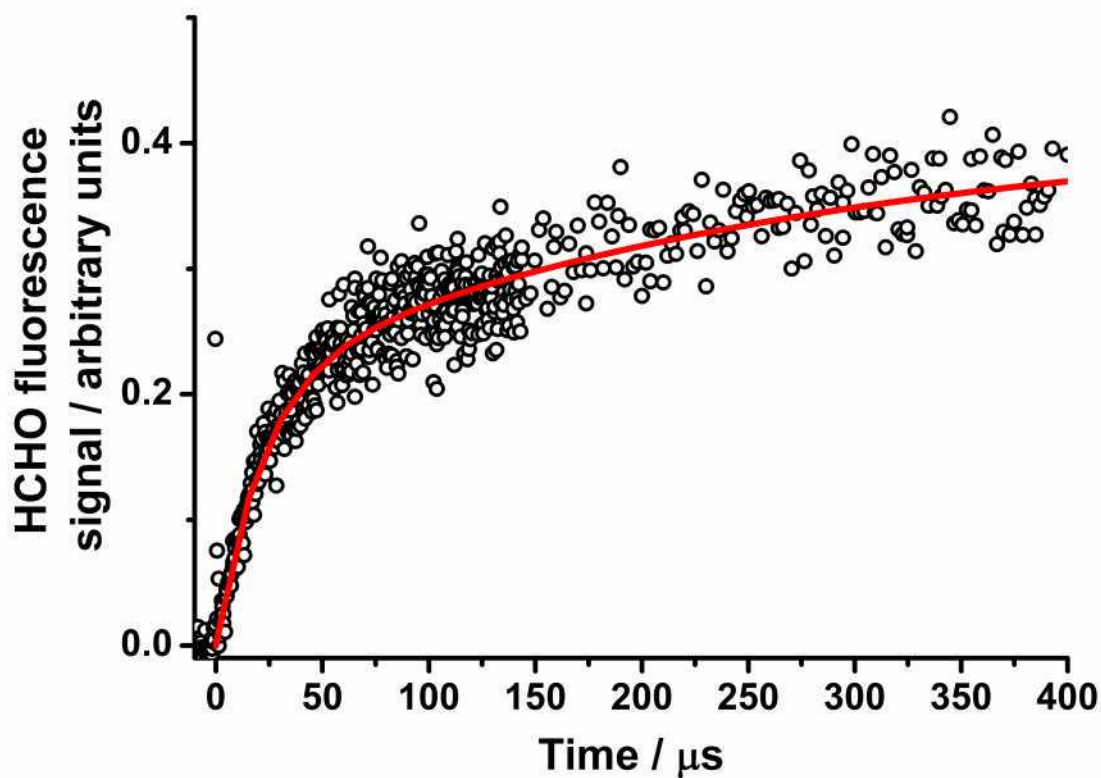


504

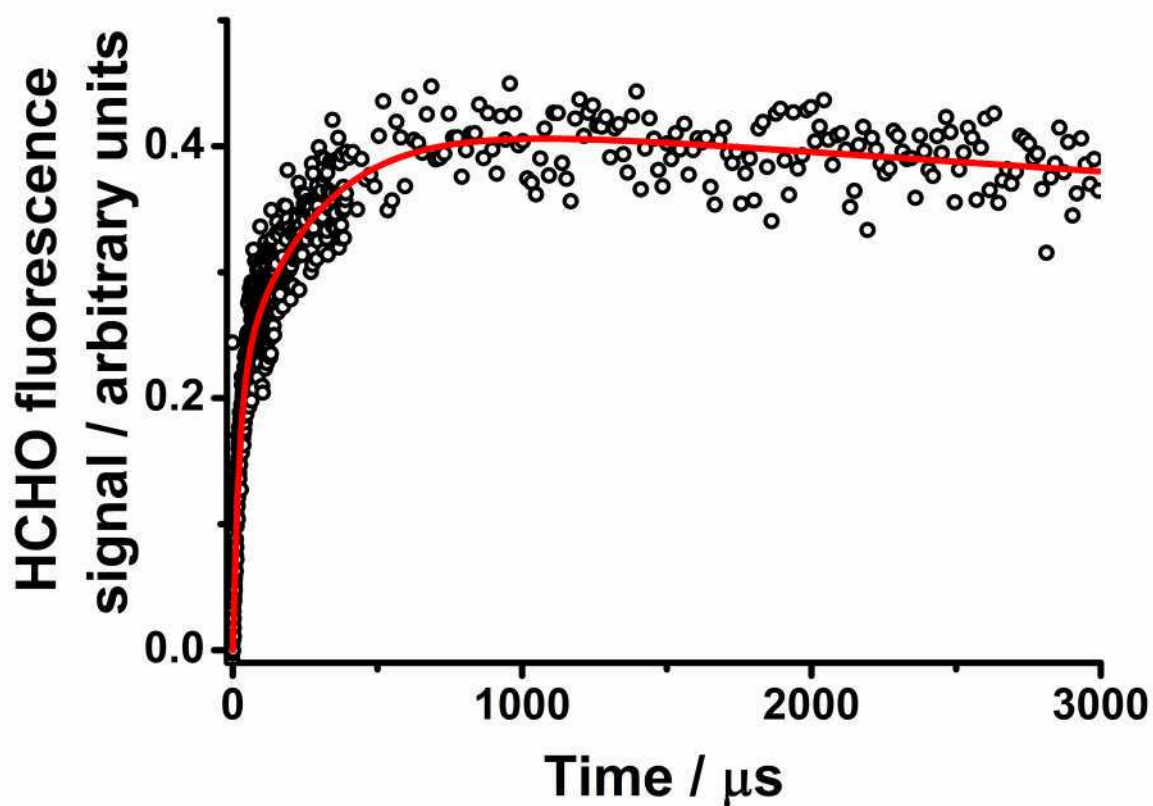


505

506 Figure 3: a) Pseudo-first-order rate coefficients (k') at 1.5 Torr, derived from fits to Equation 3, for the
 507 decay of the CH_2OO ion signal ($m/z = 46$, ionised using VUV radiation at 118 nm) following photolysis of
 508 $\text{CH}_2\text{I}_2/\text{O}_2/\text{N}_2$ in the presence of SO_2 . Error bars are 1σ . The fit to the data (shown in red) gives the
 509 bimolecular rate coefficient for $\text{CHOO} + \text{SO}_2$ (k_7); b) Pseudo-first-order rate coefficients (k') for the rapid
 510 HCHO production at 250 Torr following photolysis of $\text{CH}_2\text{I}_2/\text{O}_2/\text{N}_2$ in the presence of SO_2 derived from fits
 511 to Equation 2. Error bars are 1σ . The fit to the data (shown in red) gives the bimolecular rate coefficient
 512 for $\text{CHOO} + \text{SO}_2$ (k_7).

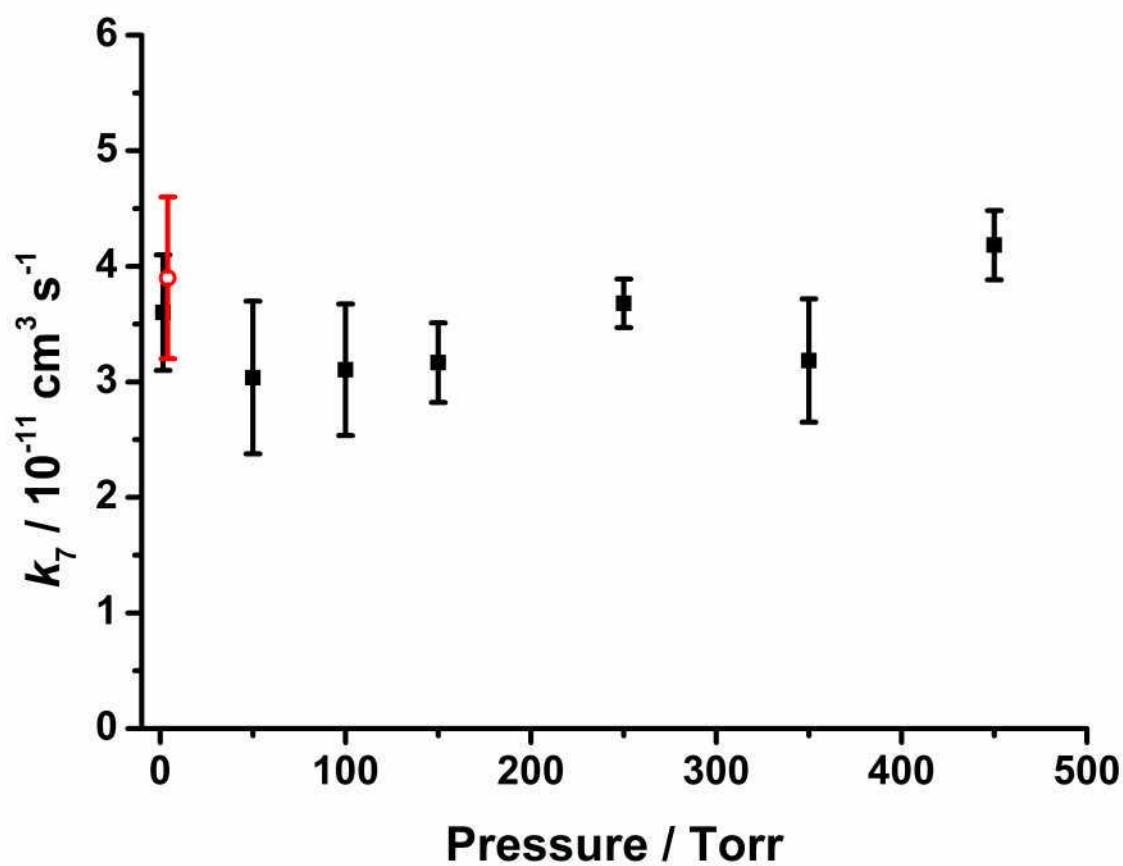


513

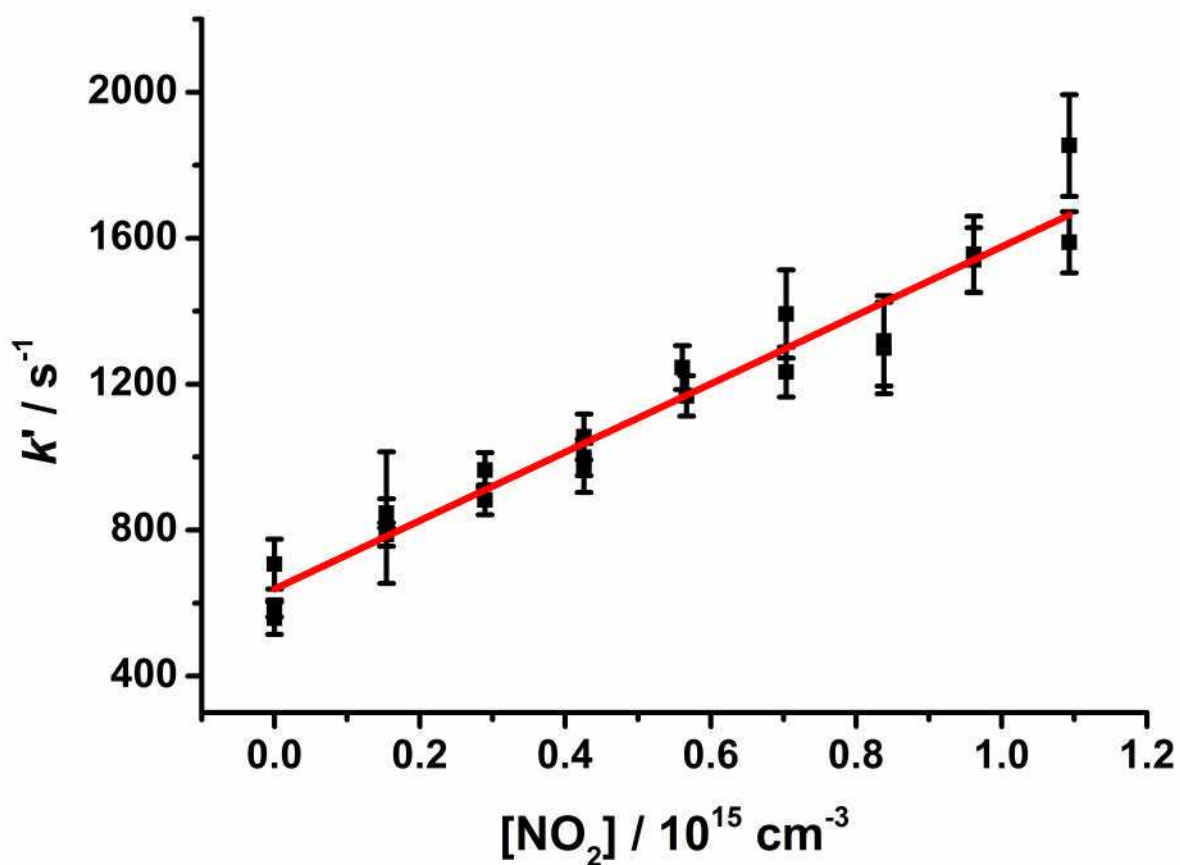


514

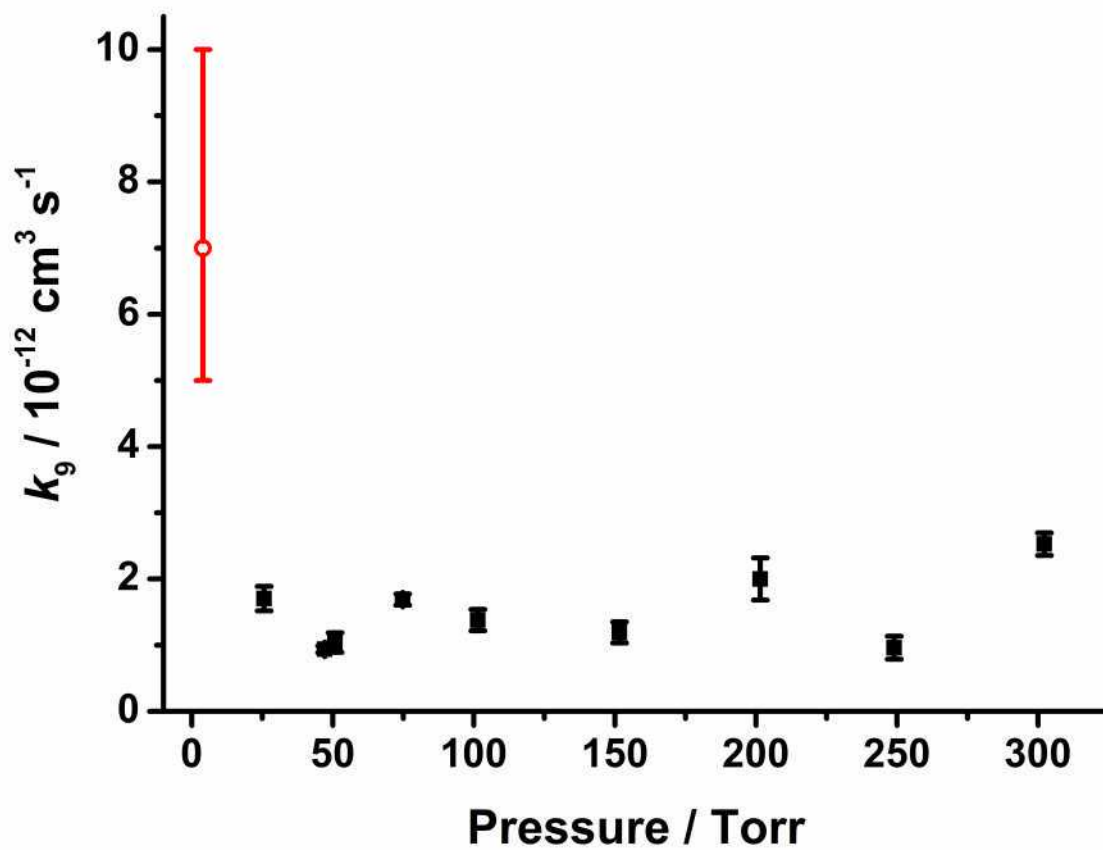
515 Figure 4: HCHO fluorescence signals at 250 Torr following photolysis of $\text{CH}_2\text{I}_2/\text{O}_2/\text{N}_2$ in the presence of
 516 SO_2 , with the fit to Equation 2 (solid red lines). The inset panel shows the evolution of the signal to longer
 517 times. For these data, $k'_{g1} = (45500 \pm 2240) \text{ s}^{-1}$; $k'_{g2} = (3580 \pm 280) \text{ s}^{-1}$; $k_{\text{loss}} = (40 \pm 9) \text{ s}^{-1}$; $f = (0.49 \pm 0.01)$;
 518 $S_0 = (0.43 \pm 0.01)$.



519
520 Figure 5: Bimolecular rate coefficients for $\text{CH}_2\text{OO} + \text{SO}_2$ (k_7) as a function of pressure. Error bars are 1σ .
521 The plot includes results from the PIMS experiments (at 1.5 Torr) and the LIF experiments (pressures ≥ 50
522 Torr). The data point shown by the red open circle is that determined by Welz *et al.*¹⁰



523
 524 Figure 6: Pseudo-first-order rate coefficients (k') for HCHO production at 50 Torr, derived from fits to
 525 Equation 1, following photolysis of $\text{CH}_2\text{I}_2/\text{O}_2/\text{N}_2$ in the presence of NO_2 . Error bars are 1σ . The fit to the
 526 data (shown in red) gives the bimolecular rate coefficient for $\text{CH}_2\text{OO} + \text{NO}_2$ (k_9).



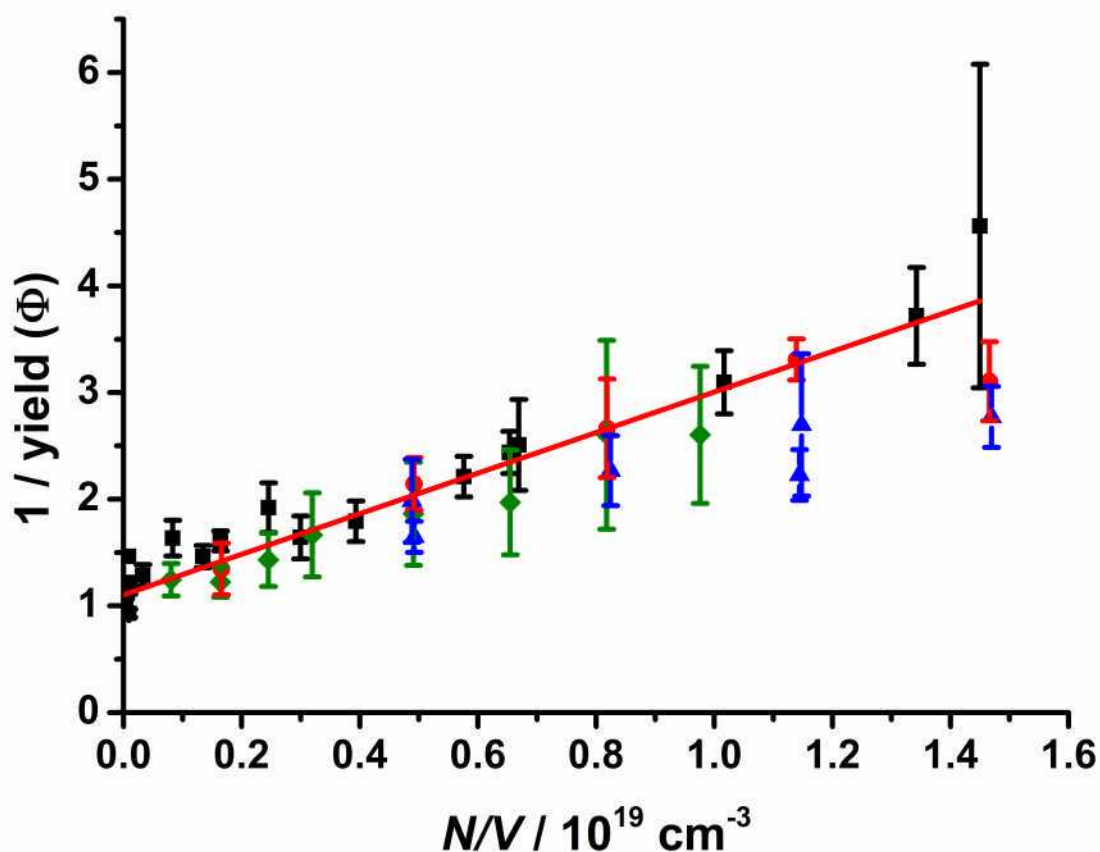
527

528

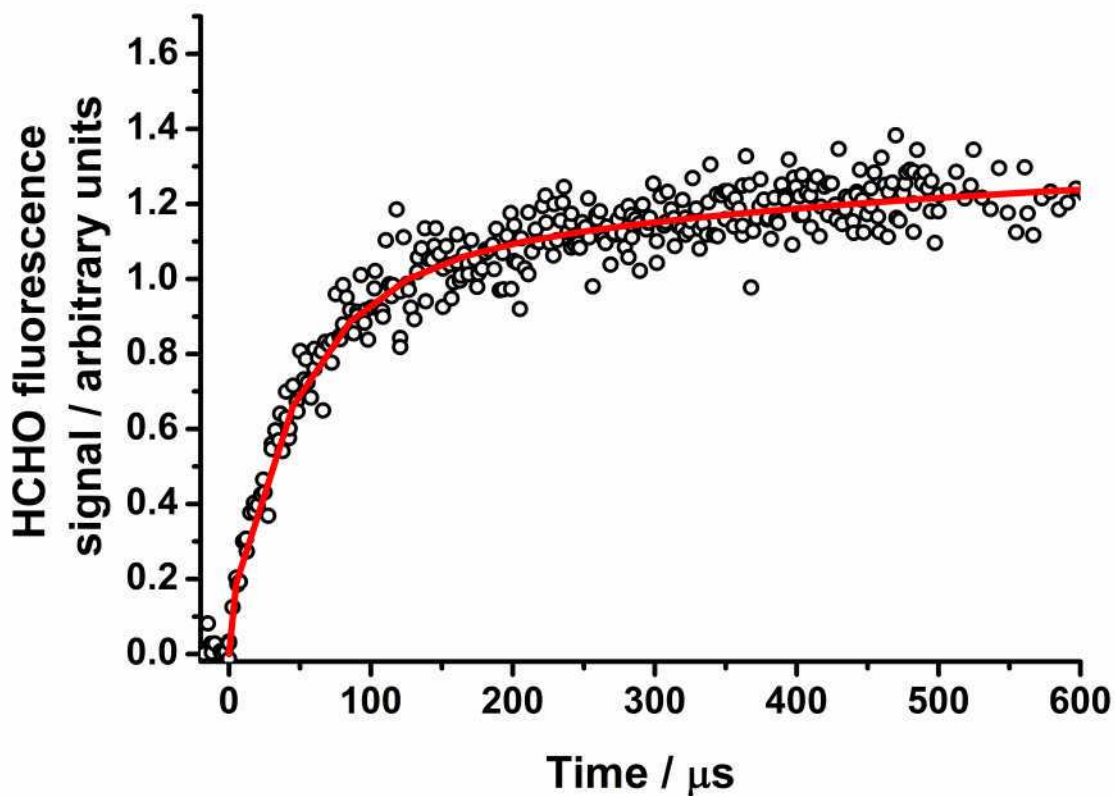
Figure 7: Bimolecular rate coefficients for $\text{CH}_2\text{OO} + \text{NO}_2$ (k_9) as a function of pressure. Error bars are 1σ .

529

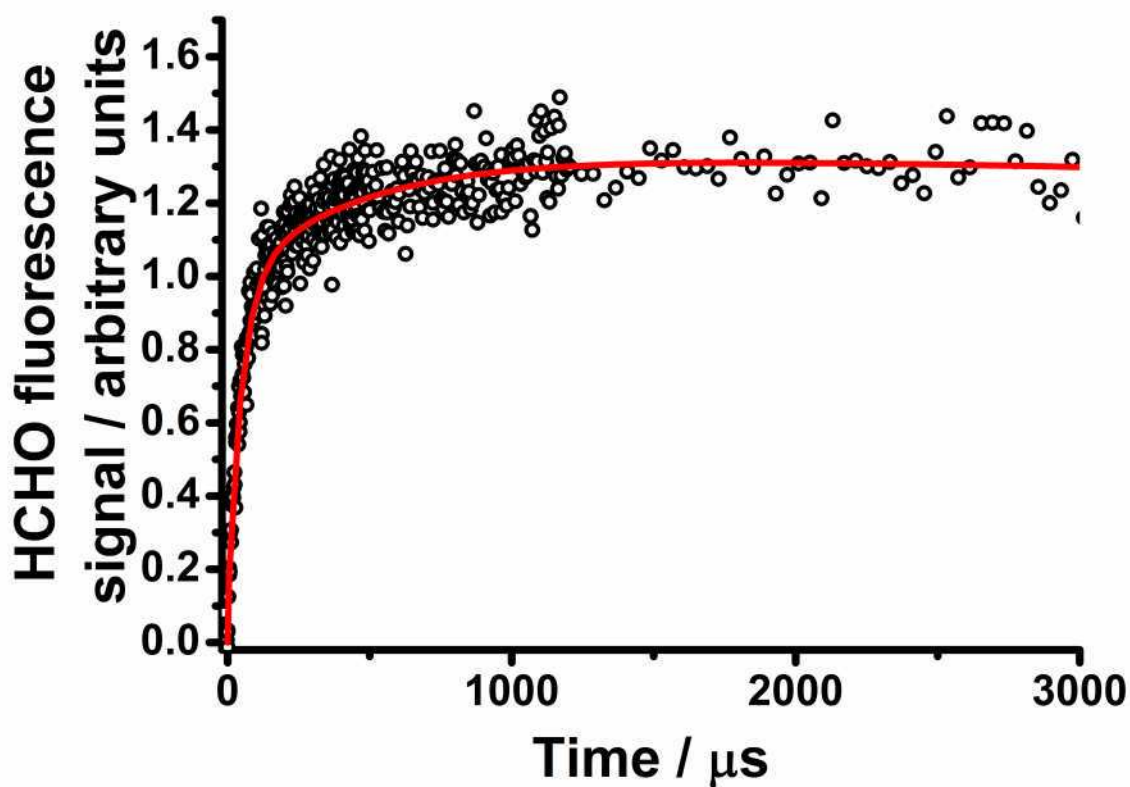
The data point shown by the red open circle is that determined by Welz *et al.*¹⁰



530
 531 Figure 8: Stern-Volmer plot showing (inverse) yields of CH₂OO as a function of pressure from the reaction
 532 of CH₂I with O₂. Results from our previous work are shown for experiments monitoring iodine atom
 533 production in the system (black squares), and monitoring of HCHO production in experiments with SO₂
 534 (blue triangles) and NO (red circles), with the best fit line (red). Yields of HCHO from the reaction of
 535 CH₂OO with NO₂ (this work, green diamonds), determined relative to the HCHO yields in the absence of
 536 NO₂ (*i.e.* through reactions R3-R6), suggest that there is 100 % titration of CH₂OO to HCHO in the
 537 presence of NO₂ at all pressures (*i.e.* there is no stabilisation of reaction products), and that there is little
 538 production of HCHO from CH₂IO₂ in the system. The fit to our previous work (comprising data from the I
 539 atom, NO and SO₂ experiments) gives an intercept of 1.10 ± 0.23 and a slope of $(1.90 \pm 0.22) \times 10^{-19} \text{ cm}^3$.
 540 The NO₂ experiments give an intercept of 1.05 ± 0.12 and a slope of $(1.70 \pm 0.18) \times 10^{-19} \text{ cm}^3$.

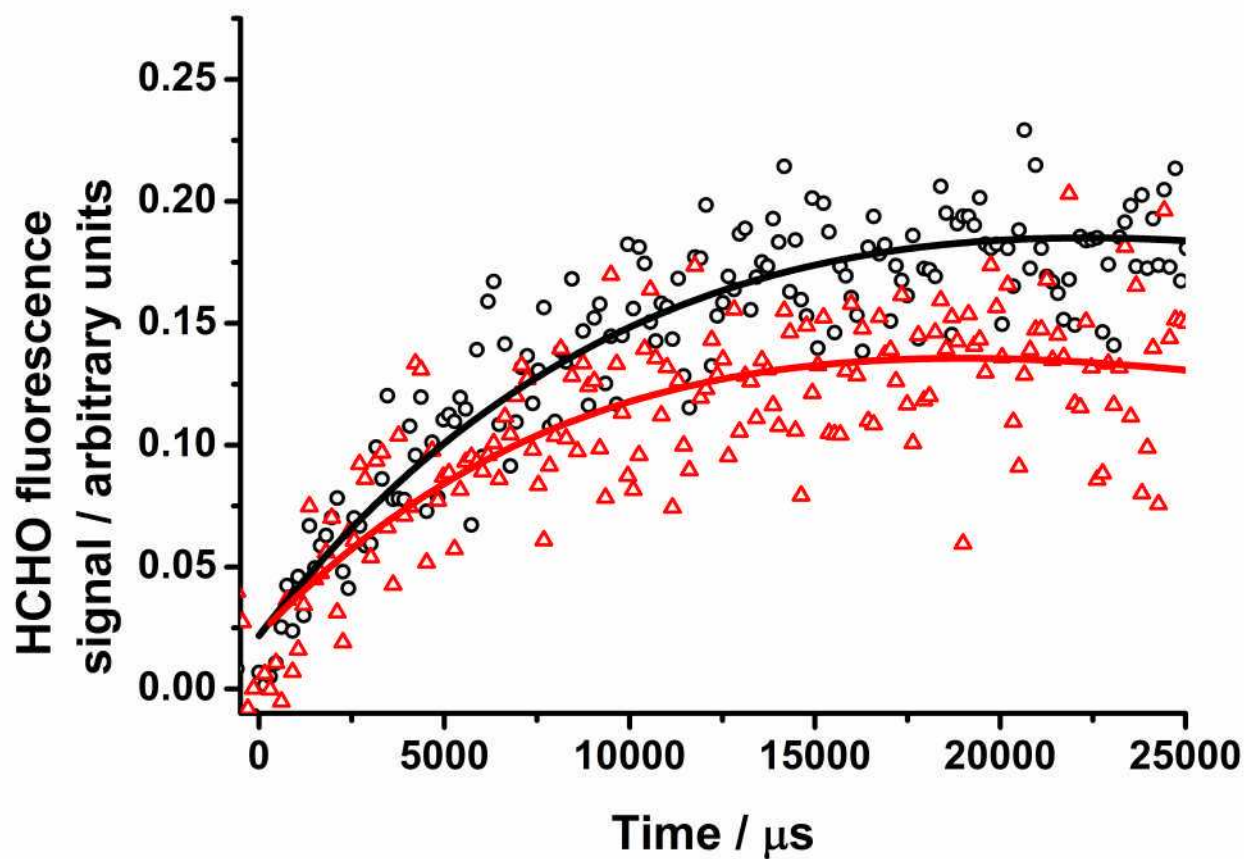


541



542

543 Figure 9: HCHO fluorescence signals at 250 Torr following photolysis of $\text{CH}_2\text{I}_2/\text{O}_2/\text{N}_2$ in the presence of
 544 NO, with the fit to Equation 2 (solid red lines). The inset panel shows the evolution of the signal to longer
 545 times. For these data, $k'_{g1} = (24800 \pm 1400) \text{ s}^{-1}$; $k'_{g2} = (2660 \pm 320) \text{ s}^{-1}$; $k_{\text{loss}} = (10 \pm 2) \text{ s}^{-1}$; $f = (0.70 \pm 0.02)$;
 546 $S_0 = (1.33 \pm 0.01)$.



547

548

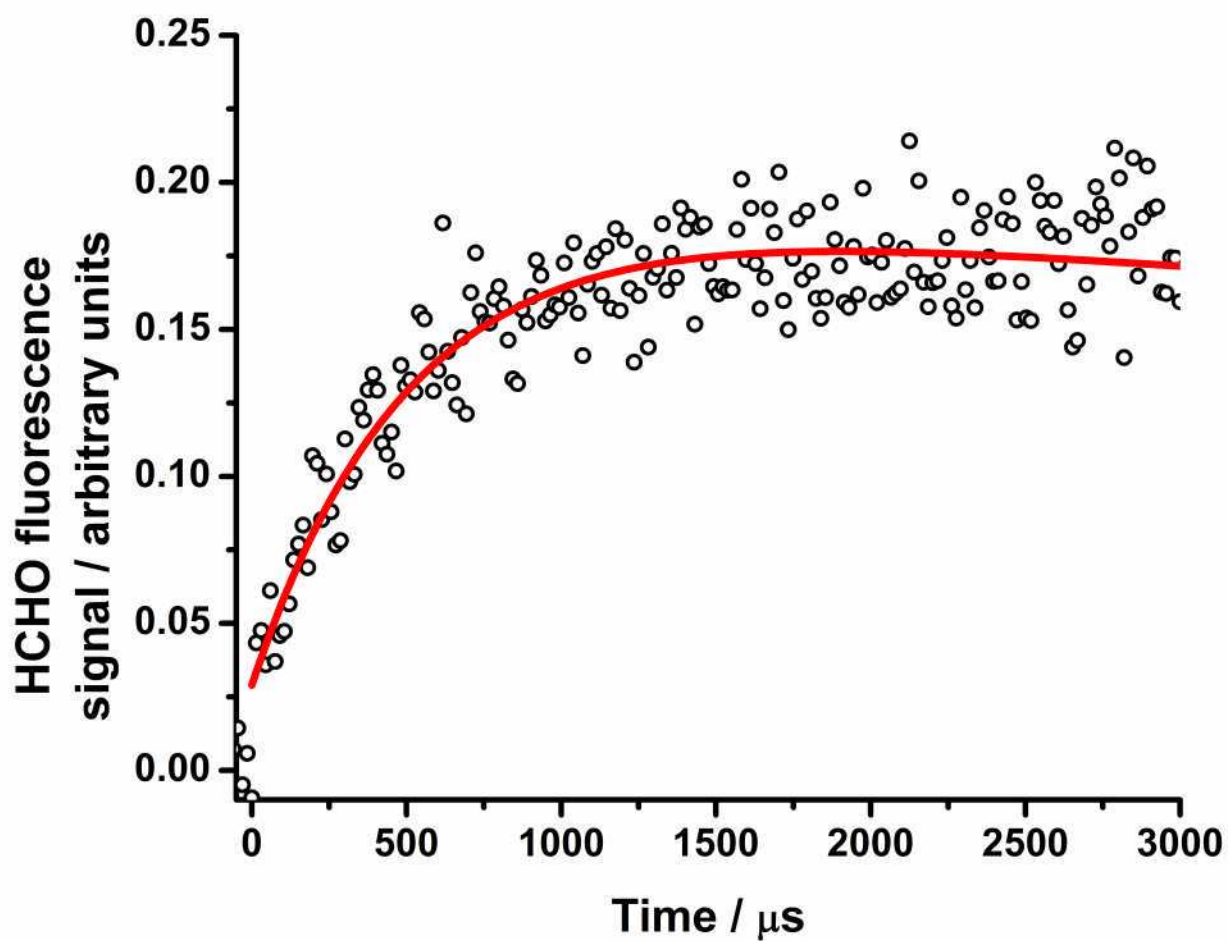
549

550

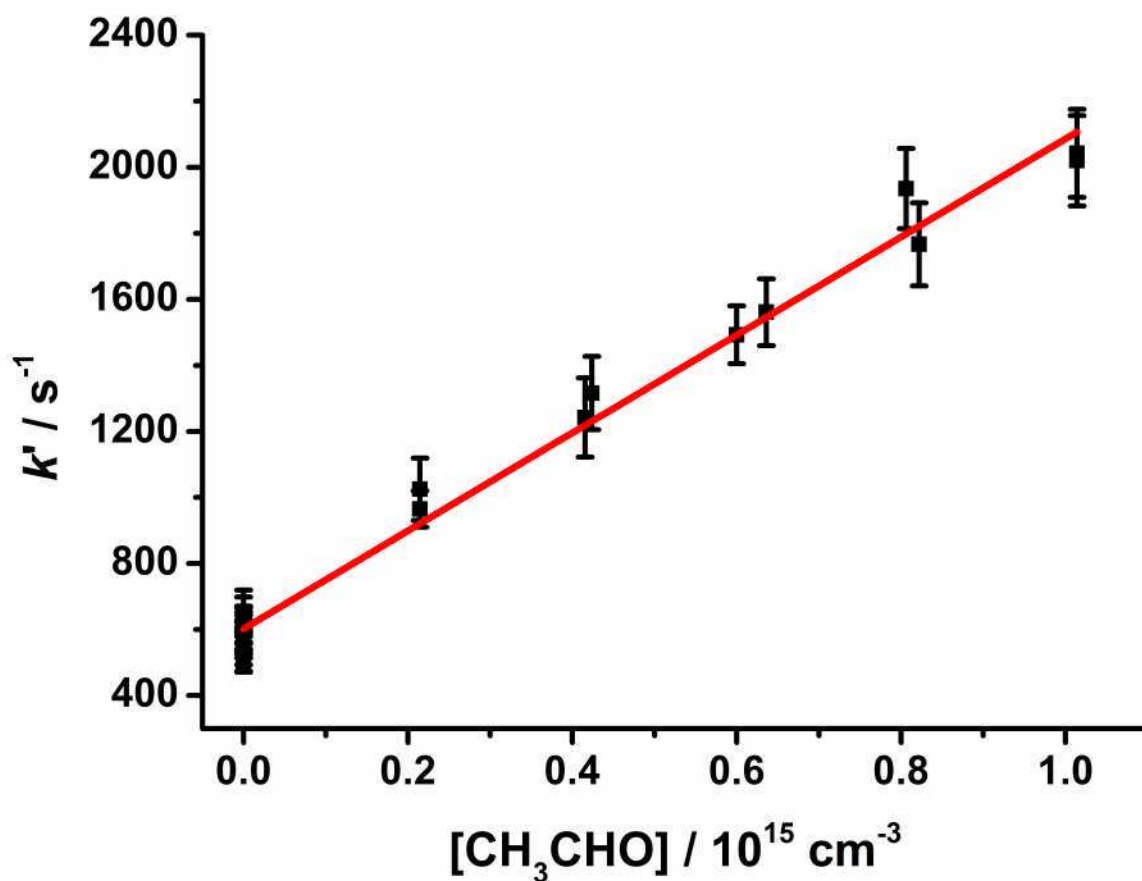
551

552

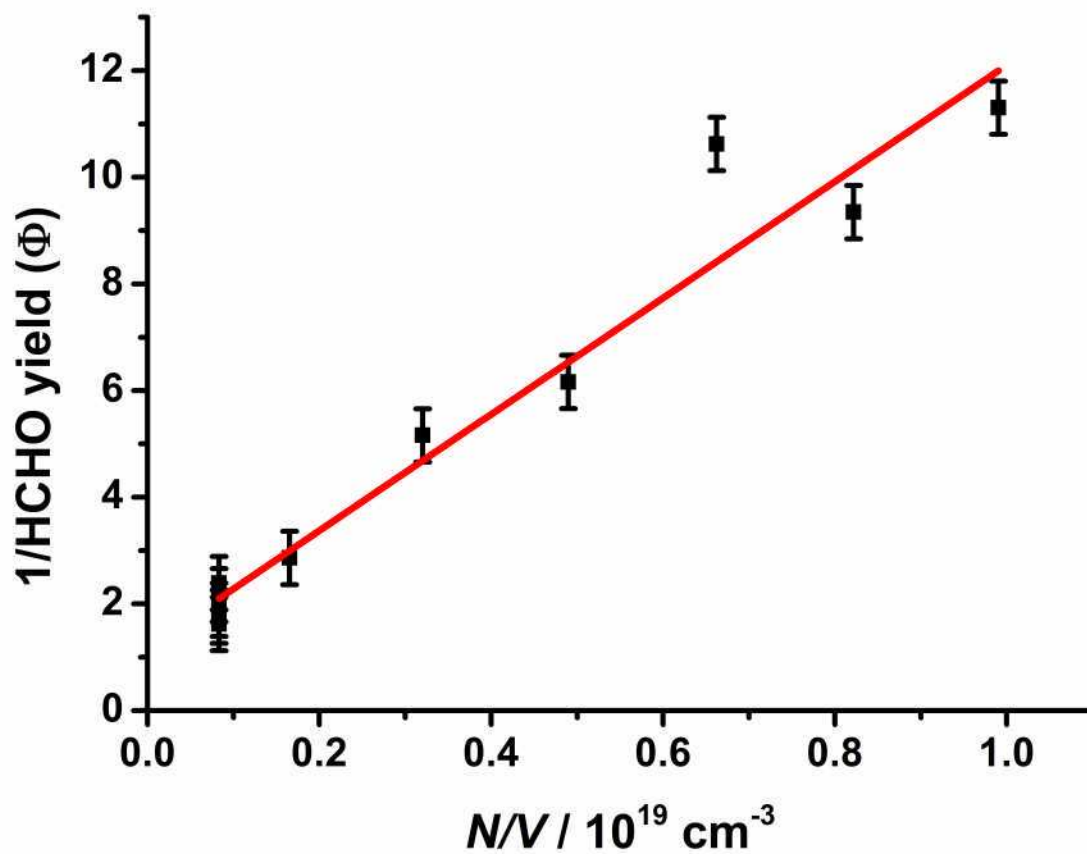
Figure 10: HCHO fluorescence signals at 200 Torr following photolysis of $\text{CH}_2\text{I}_2/\text{O}_2/\text{N}_2$ in the absence (black open circles) and presence of water vapour (red open triangles), with the fits to Equation 1 (solid lines). The differences in the amplitude of the signal result from the quenching of the fluorescence signal by H_2O . For these data, $k' = (41 \pm 15) \text{ s}^{-1}$ in the absence of water vapour and $k' = (52 \pm 13) \text{ s}^{-1}$ in the presence of water vapour.



553
554 Figure 11: HCHO fluorescence signals at 25 Torr following photolysis of $\text{CH}_2\text{I}_2/\text{O}_2/\text{N}_2$ in the presence of
555 CH_3CHO , with the fit to Equation 1 (solid red line). For these data, $k' = (2040 \pm 120) \text{ s}^{-1}$.



556
 557 Figure 12: Pseudo-first-order rate coefficients (k') for HCHO production at 25 Torr, derived from fits to
 558 Equation 1, following photolysis of $\text{CH}_2\text{I}_2/\text{O}_2/\text{N}_2$ in the presence of CH_3CHO . Error bars are 1σ . The fit to
 559 the data (shown in red) gives the bimolecular rate coefficient for $\text{CH}_2\text{OO} + \text{CH}_3\text{CHO}$ (k_{13}).



560 Figure 13: Stern-Volmer analysis for HCHO yields from $\text{CH}_2\text{OO} + \text{CH}_3\text{CHO}$ (R13) (corrected for HCHO
 561 production from CH_2IO_2 chemistry) as a function of total pressure, with the fit to the data (red). Error bars
 562 are 1σ .
 563

564

565

- 567 1. D. Johnson and G. Marston, *Chem. Soc. Rev.*, 2008, **37**, 699–716.
- 568 2. C. A. Taatjes, D.E. Shallcross, C. Percival, *Phys. Chem. Chem. Phys.*, 2013, DOI: **10.1039/C3CP52842A**.
- 569 3. N. M. Donahue, G. T. Drozd, S. A. Epstein, A. A. Presto and J. H. Kroll, *Physical Chemistry Chemical Physics*,
570 2011, **13**, 10848-10857.
- 571 4. M. S. Alam, M. Camredon, A. R. Rickard, T. Carr, K. P. Wyche, K. E. Hornsby, P. S. Monks and W. J. Bloss,
572 *Phys. Chem. Chem. Phys.*, 2011, **12**, 11002-11015.
- 573 5. L. Vereecken, *Science*, 2013, **340**, 154-155.
- 574 6. T. L. Malkin, A. Goddard, D. E. Heard and P. W. Seakins, *Atmospheric Chemistry and Physics*, 2010, **10**, 1441-
575 1459.
- 576 7. D. E. Heard, L. J. Carpenter, D. J. Creasey, J. R. Hopkins, J. D. Lee, A. C. Lewis, M. J. Pilling, P. W. Seakins, N.
577 Carslaw and K. M. Emmerson, *Geophys. Res. Lett.*, 2004, **31**, L18112.
- 578 8. R. M. Harrison, J. Yin, R. M. Tilling, X. Cai, P. W. Seakins, J. R. Hopkins, D. L. Lansley, A. C. Lewis, M. C. Hunter,
579 D. E. Heard, L. J. Carpenter, D. J. Creasey, J. D. Lee, M. J. Pilling, N. Carslaw, K. M. Emmerson, A. Redington,
580 R. G. Derwent, D. Ryall, G. Mills and S. A. Penkett, *Sci. Total Environ.*, 2006, **360**, 5-25.
- 581 9. D. Stone, L. K. Whalley and D. E. Heard, *Chemical Society Reviews*, 2012, **41**, 6348-6404.
- 582 10. O. Welz, J. D. Savee, D. L. Osborn, S. S. Vasu, C. J. Percival, D. E. Shallcross and C. A. Taatjes, *Science*, 2012,
583 **335**, 204-207.
- 584 11. C. A. Taatjes, O. Welz, A. J. Eskola, J. D. Savee, D. L. Osborn, E. P. F. Lee, J. M. Dyke, D. W. K. Mok, D. E.
585 Shallcross and C. J. Percival, *Phys. Chem. Chem. Phys.*, 2012, **14**, 10391-10400.
- 586 12. C. A. Taatjes, O. Welz, A. J. Eskola, J. D. Savee, A. M. Scheer, D. E. Shallcross, B. Rotavera, E. P. F. Lee, J. M.
587 Dyke, D. K. W. Mok, D. L. Osborn and C. J. Percival, *Science*, 2013, **340**, 177-180.
- 588 13. L. Vereecken, H. Harder and A. Novelli, *Physical Chemistry Chemical Physics*, 2012, **14**, 14682-14695.
- 589 14. M. Boy, D. Mogensen, S. Smolander, L. Zhou, T. Nieminen, P. Paasonen, C. Plass-Duelmer, M. Sipila, T.
590 Petaja, L. Mauldin, H. Berresheim and M. Kulmala, *Atmospheric Chemistry and Physics*, 2013, **13**, 3865-3879.
- 591 15. J. R. Pierce, M. J. Evans, C. E. Scott, S. D. D'Andrea, D. K. Farmer, E. Swietlicki and D. V. Spracklen,
592 *Atmospheric Chemistry and Physics*, 2013, **13**, 3163-3176.
- 593 16. G. Sarwar, K. Fahey, R. Kwok, R. C. Gilliam, S. J. Roselle, R. Mathur, J. Xue, J. Yu and W. P. L. Carter,
594 *Atmospheric Environment*, 2013, **68**, 186-197.
- 595 17. C. J. Percival, Welz, O., Eskola, A.J., Savee, J.D., Osborn, D.L., Topping, D.O., Lowe, D., Utembe, S.R., Bacak,
596 A., McFiggans, G., Cooke, M.C., Xiao, P., Archibald, A.T., Jenkin, M.E., Derwent, R.G., Riipinen, I., Mok,
597 D.W.K., Lee, E.P.F., Dyke, J.M., Taatjes, C.A., Shallcross, D.E., *Faraday Discuss*, 2013, DOI:
598 **10.1039/C3FD00048F**
- 599 18. C. A. Taatjes, G. Meloni, T. M. Selby, A. J. Trevitt, D. L. Osborn, C. J. Percival and D. E. Shallcross, *J. Am.*
600 *Chem. Soc.*, 2008, **130**, 11883-11885.
- 601 19. Y.-T. Su, Y.-H. Huang, H. A. Witek and Y.-P. Lee, *Science*, 2013, **340**, 174-176.
- 602 20. J. M. Beames, F. Liu, L. Lu and M. I. Lester, *J. Am. Chem. Soc.*, 2012, **134**, 20045-20048.
- 603 21. B. Ouyang, M.W. McLeod, R.L. Jones, W.J. Bloss, *Phys. Chem. Chem. Phys.*, 2013, **15**, 17070-17075.
- 604 22. A. Jalan, Allen, J.W., Green, W.H., *Phys. Chem. Chem. Phys.*, 2013, **15**, 16841-16852.
- 605 23. R. L. Mauldin, III, T. Berndt, M. Sipilae, P. Paasonen, T. Petaja, S. Kim, T. Kurten, F. Stratmann, V. M.
606 Kerminen and M. Kulmala, *Nature*, 2012, **488**, 193-+.
- 607 24. T. Kurten, J. R. Lane, S. Jorgensen and H. G. Kjaergaard, *Journal of Physical Chemistry A*, 2011, **115**, 8669-
608 8681.
- 609 25. H. Huang, A. J. Eskola and C. A. Taatjes, *J. Phys. Chem. Lett.*, 2012, **3**, 3399-3403.
- 610 26. D. Stone, Blitz, M., Daubney, L., Ingham, T., Seakins, P., *Phys. Chem. Chem. Phys.*, 2013, **15**, 19119-19124.
- 611 27. H. Huang, B. Rotavera, A.J. Eskola, C.A. Taatjes, *J. Phys. Chem. Lett.*, 2013, **4**, 3824-3824.
- 612 28. C. M. Roehl, J. B. Burkholder, G. K. Moortgat, A. R. Ravishankara and P. Crutzen, *J. Geophys. Res. Atmos.*,
613 1997, **102**, 12,819 -812,829
- 614 29. L. J. Carpenter, W. T. Sturges, S. A. Penkett, P. S. Liss, B. Alicke, K. Hebestreit and U. Platt, *J. Geophys. Res.*
615 *Atmos.*, 1999, **104**, 1679-1689.
- 616 30. L. J. Carpenter, *Chem. Rev.*, 2003, **103**, 4953-4962.
- 617 31. L. J. Carpenter, S. D. Archer and R. Beale, *Chem. Soc. Rev.*, 2012, **41**, 6473-6506.
- 618 32. T. J. Gravestock, M. A. Blitz, W. J. Bloss and D. E. Heard, *Chem. Phys. Chem*, 2010, **11**, 3928-3941.
- 619 33. R. A. Cox, *J. Phys. Chem.*, 1972, **76**, 814-&.
- 620 34. J. L. Jourdain, G. Lebras and J. Combourieu, *Int. J. Chem. Kinet.*, 1979, **11**, 569-577.

- 621 35. K. J. Hughes, M. A. Blitz, M. J. Pilling and S. H. Robertson, *Proc. Combust. Inst.*, 2002, **29**, 2431-2437.
622 36. D. T. Co, T. F. Hanisco, J. G. Anderson and F. N. Keutsch, *J. Phys. Chem. A*, 2005, **109**, 10675-10682.
623 37. M. A. Blitz, A. Goddard, T. Ingham and M. J. Pilling, *Review of Scientific Instruments*, 2007, **78**.
624 38. M. Teresa Baeza-Romero, M. A. Blitz, A. Goddard and P. W. Seakins, *International Journal of Chemical
625 Kinetics*, 2012, **44**, 532-545.
626 39. G. Hancock and V. Haverd, *Chem. Phys. Lett.*, 2003, **372**, 288-294.
627 40. H. M. Su, W. T. Mao and F. N. Kong, *Chem. Phys. Lett.*, 2000, **322**, 21-26.
628 41. U. Bley, F. Temps, H. G. Wagner and M. Wolf, *Ber. Bunsen-Ges. Phys. Chem. Chem. Phys.*, 1992, **96**, 1043-
629 1048.
630 42. R. A. Alvarez and C. B. Moore, *J. Phys. Chem.*, 1994, **98**, 174-183.
631 43. M. A. Blitz, C. Kappler, M. J. Pilling and P. W. Seakins, *Zeitschrift Fur Physikalische Chemie-International
632 Journal of Research in Physical Chemistry & Chemical Physics*, 2011, **225**, 957-967.
633 44. A. J. Eskola, D. Wojcik-Pastuszka, E. Ratajczak and R. S. Timonen, *Journal of Physical Chemistry A*, 2006, **110**,
634 12177-12183.
635 45. A. J. Eskola, D. Wojcik-Pastuszka, E. Ratajczak and R. S. Timonen, *Phys. Chem. Chem. Phys.*, 2006, **8**, 1416-
636 1424.
637 46. A. Masaki, S. Tsunashima and N. Washida, *J. Phys. Chem.*, 1995, **99**, 13126-13131.
638 47. J. C. Ianni, *Kintecus, Windows Version 2.80*, www.kintecus.com, 2002.
639 48. P. D. Lightfoot, R. A. Cox, J. N. Crowley, M. Destriau, G. D. Hayman, M. E. Jenkin, G. K. Moortgat and F. Zabel,
640 *Atmos. Environ. A*, 1992, **26**, 1805-1961.
641 49. R. Atkinson, D. L. Baulch, R. A. Cox, J. N. Crowley, R. F. Hampson, R. G. Hynes, M. E. Jenkin, M. J. Rossi and J.
642 Troe, *Atmospheric Chemistry and Physics*, 2006, **6**, 3625-4055.
643 50. O. Horie, C. Schafer and G. K. Moortgat, *International Journal of Chemical Kinetics*, 1999, **31**, 261-269.

644

645